corresponding to length of n-alkyl side chain (Fig. 2A). Compounds **10** and **11** exhibit EC_{50} values of 2.7 and 5.9 μM, respectively, SI values of 29.6 and 9.80, respectively, and *Clog P* values of 4.90 and 5.96, respectively, suggesting that high hydrophobic property of n-alkyl side chain decreases anti-HCV activity. The appropriate *Clog P* value of caffeic acid ester containing unsaturated side chain may be around 5.

Dihydrocaffeic acid methyl ester (compound **12**) showed less activity than caffeic acid methyl ester (compound **7**) regardless of values of *Clog P* value and CC_{50}, suggesting that the alpha, beta-unsaturated part attached to ester affects the anti-HCV activity level (Table 3 and Figure S3).

We further examined the effect of the hydroxyl groups on the aromatic ring on HCV replication (Table 4 and Figure S4). The EC_{50} values of *O*-methylated caffeic acid n-octyl esters (compounds **13** and **14**) were higher than that of compound **10**. Compounds **15** including 3, 4-di-*O*-methylated caffeic acid n-octyl ester exhibited higher EC_{50} than values of compounds **10**, **13** and **14**. However, addition of a third hydroxyl group to 3, 4, 5-trihydroxy derivative (compound **16**) of compound **10** resulted in a reduction of anti-HCV activity. Furthermore, *Clog P* values of compound **10**, **13**, **14, 15** and **16** were not correlated with anti-HCV activity (EC_{50} value) (Fig. 2B). These results suggest that the catechol moiety plays an important role in anti-HCV activity, and that the 4-hydroxy moiety is more important for the activity than the 3-hydroxy moiety.

Thus, compound **10**, which exhibits the lowest EC_{50} value and the highest SI value, is the most effective compound among CAPE analogues used in this study.

Effect of CAPE derivatives on virus production

The structure of compound **10** is shown in Fig. 3A. Treatment with compound **10** reduced HCV replication and NS3 protein in a dose-dependent manner at a higher anti-HCV level than

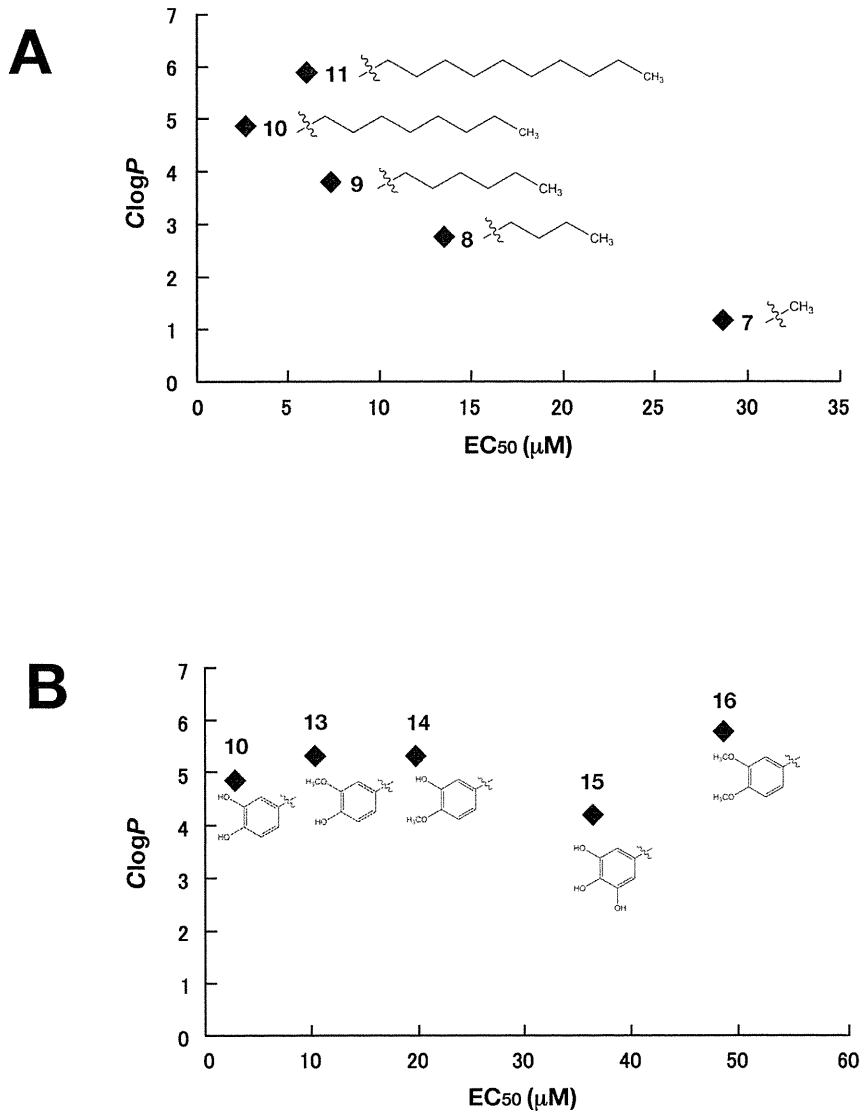

Figure 2. Correlation between the inhibitory effect on HCV replication *and* Clog *P* of CAPE analogues. Values of *x*-axis indicate EC_{50} values of CAPE analogues, while values of *y*-axis show Clog *P* values. (A) Correlation between the inhibitory effect on HCV replication and Clog *P* of CAPE analogues (Compound 7–11). (B) Correlation between the inhibitory effect on HCV replication and Clog *P* of CAPE analogues (Compound 10 and 13–16).
doi:10.1371/journal.pone.0082299.g002

Table 2. Effect of caffeic acid esters **7, 9–14**, including **1**, on HCV replication.

Compound No.	R	EC_{50} [a] (μM)	CC_{50} [b] (μM)	SI [c]	*Clog P* [d]
7	CH_3	28.6±1.2	122.1±5.0	4.2	1.20
8	C_4H_9	13.5±2.1	39.0±1.1	2.9	2.79
9	C_6H_{13}	7.3±0.2	37.6±1.2	5.1	3.85
10	C_8H_{17}	2.7±0.1	71.7±8.5	26.6	4.90
11	$C_{10}H_{21}$	5.9±0.9	57.9±2.9	9.8	5.96
1	$(CH_2)_2Ph$	9.0±0.7	136.1±1.9	17.9	3.30

The basic structure and side moieties are shown in Figure S2.
a: Fifty percent effective concentration based on the inhibition of HCV replication.
b: Fifty percent cytotoxicity concentration based on the reduction in cell viability.
c: Selectivity index (CC_{50}/EC_{50}).
d: Determined with ChemDraw software (Chem Bio Office Ultra, 2008).
doi:10.1371/journal.pone.0082299.t002

compound **1** (Figs. 3B and C), but not effect enzymatic activities of firefly and *Renilla* luciferases (Fig. 3D) and IRES-dependent translation (Fig. 3E), suggesting that inhibition of HCV replication by compound **10** is not due to offtarget effect. We evaluated the inhibitory effect of compound **10** on three different subgenomic replicon cell lines (1b: N strain, Con1 strain, 2a: JFH-1 strain) and one full genome replicon cell line (1b: O strain). Compound **10** inhibited the viral replication of all replicon cell lines at similar level, and exhibited the lowest EC_{50} value of 1.0 μM and an SI value of 63.1 by using Con1 replicon cells (Table 5). We next examined the effect of compound **10** on virus production by using HCVcc, since subgenomic replicon mimics HCV replication, but not the whole viral cycle. The Huh7 OK1 cell line, which is highly permissive to the HCV JFH1 strain [22], was infected with HCVcc and then treated with compound **10** at 24 h post-infection. The supernatant was harvested 72 h post-infection from the culture supernatant and then the RNA that prepared from the supernatant was estimated by real time qRT-PCR. Figure 3F shows that treatment with compound **10** reduced HCV viral production (EC_{50} = 1.8±0.4 μM) in a similar way to the data obtained by using a replicon cell line. To clarify whether or not compound **10** inhibited HCV replication via interferon-signaling pathway, we analyzed ISRE activity and the expression of interferon stimulated gene (ISG) by using reporter assay and RT-PCR, respectively. The replicon cells were harvested at 48 h post-treatment. There were no significant effects of compound **1**, **6** and **10** on ISRE-promoter activities, while interferon alpha 2b significantly enhanced it as a positive control (Fig.4 A). The data of the RT-PCR analysis showed that the transcriptional expressions of ISGs including Mx1, MxA, IFIT4, ISG15, OAS1, OAS2, and OAS3 were induced with interferon alpha 2b, but not with compound **1**, **6** and **10** (Fig. 4B). These data suggest that the CAPE derivatives have an inhibitory effect on virus production and replication, irrespective of interferon signaling induction.

Synergistic effect of caffeic acid n-octyl ester on interferon and direct-acting antiviral agents

To estimate the effects of drug combinations on anti-HCV activity, we examined the antiviral activity of compound **10** in combination with IFN-α 2b, telaprevir (NS3 protease inhibitor), danoprevir (NS3 protease inhibitor), daclatasvir (NS5A inhibitor) or VX-222 (NS5B polymerase inhibitor). Con1 LUN Sb #26 replicon cells were treated with compound **10** in combination with

Table 3. Effect of caffeic acid esters **7**and **8** on HCV replication.

Compound No.	EC_{50} [a] (μM)	CC_{50} [b] (μM)	SI [c]	*Clog P* [d]
7	28.6±1.2	122.1±5.0	4.2	1.20
12	77.0±1.6	140.7±3.4	1.8	1.02

Chemical structures of both compounds are shown in Figure S3
a: Fifty percent effective concentration based on the inhibition of HCV replication.
b: Fifty percent cytotoxicity concentration based on the reduction in cell viability.
c: Selectivity index (CC_{50}/EC_{50}).
d: Determined with ChemDraw software (Chem Bio Office Ultra, 2008).
doi:10.1371/journal.pone.0082299.t003

each anti-HCV agent at various concentration rations for 72 h. The effect of each drug combination on HCV replication was analyzed by using CalcuSyn. An explanatory diagram of isobologram was shown at a right end of lower panels of Fig. 5A as described in Materials and Methods. As shown in the resulting isobologram, all plots of the calculated EC_{90} values of compound **10** with IFN-alpha 2b, daclatasvir, or VX-222 are located under the additive line, while the plots of compound **10** with telaprevir, or danoprevir are located above the additive line and closed to the additive line (Fig. 5A). Additionally, we determined the degree of inhibition for each drug combination was analyzed as the combination index (CI) calculation at 50, 75 and 90% of effective concentrations by using CalcuSyn. An explanatory diagram was shown at a right end of lower panels of Fig. 5B as described in Materials and Methods. On the basis of the CalcuSyn analysis, the combination of compound **10** with daclatasvir exhibited strong synergistic effect on inhibition of HCV replication in the replicon cells (Fig. 5B, upper middle). The combination of compound **10** with VX-222 exhibited an additive to synergistic effect, suggesting that it trends toward synergistic (Fig. 5B, upper right), and with IFN-alpha 2b exhibited an antagonistic to synergistic effect, suggesting that it trends toward synergistic (Fig. 5B, upper left). In contrast, the combination of compound **10** with telaprevir resulted in antagonistic effect (Fig. 5B, lower left), and with danoprevir resulted in an antagonistic to additive effect, suggesting it trends toward antagonistic (Fig. 5B, lower middle). These calculated data

Table 4. Effect of octyl esters **10** and **13–16** on HCV replication.

Compound No.	R^1, R^2, R^3	EC_{50} [a] (μM)	CC_{50} [b] (μM)	SI [c]	*Clog P* [d]
10	$R^1=R^2=R^3=H$	2.7±0.1	71.7±8.5	26.6	4.90
13	$R^1=CH_3$, $R^2=R^3=H$	10.2±1.1	60.3±1.6	5.9	5.35
14	$R^1=R^3=H$, $R^2=CH_3$	19.6±0.8	59.2±1.4	3	5.35
15	$R^1=R^2=CH_3$, $R^3=H$	48.5±1.7	212.4±6.9	4.4	5.82
16	$R^1=R^2=H$, $R^3=OH$	36.3±2.9	59.8±6.9	1.6	4.24

The basic structure and side moieties are shown in Figure S4.
a: Fifty percent effective concentration based on the inhibition of HCV replication.
b: Fifty percent cytotoxicity concentration based on the reduction in cell viability.
c: Selectivity index (CC_{50}/EC_{50}).
d: Determined with ChemDraw software (Chem Bio Office Ultra, 2008).
doi:10.1371/journal.pone.0082299.t004

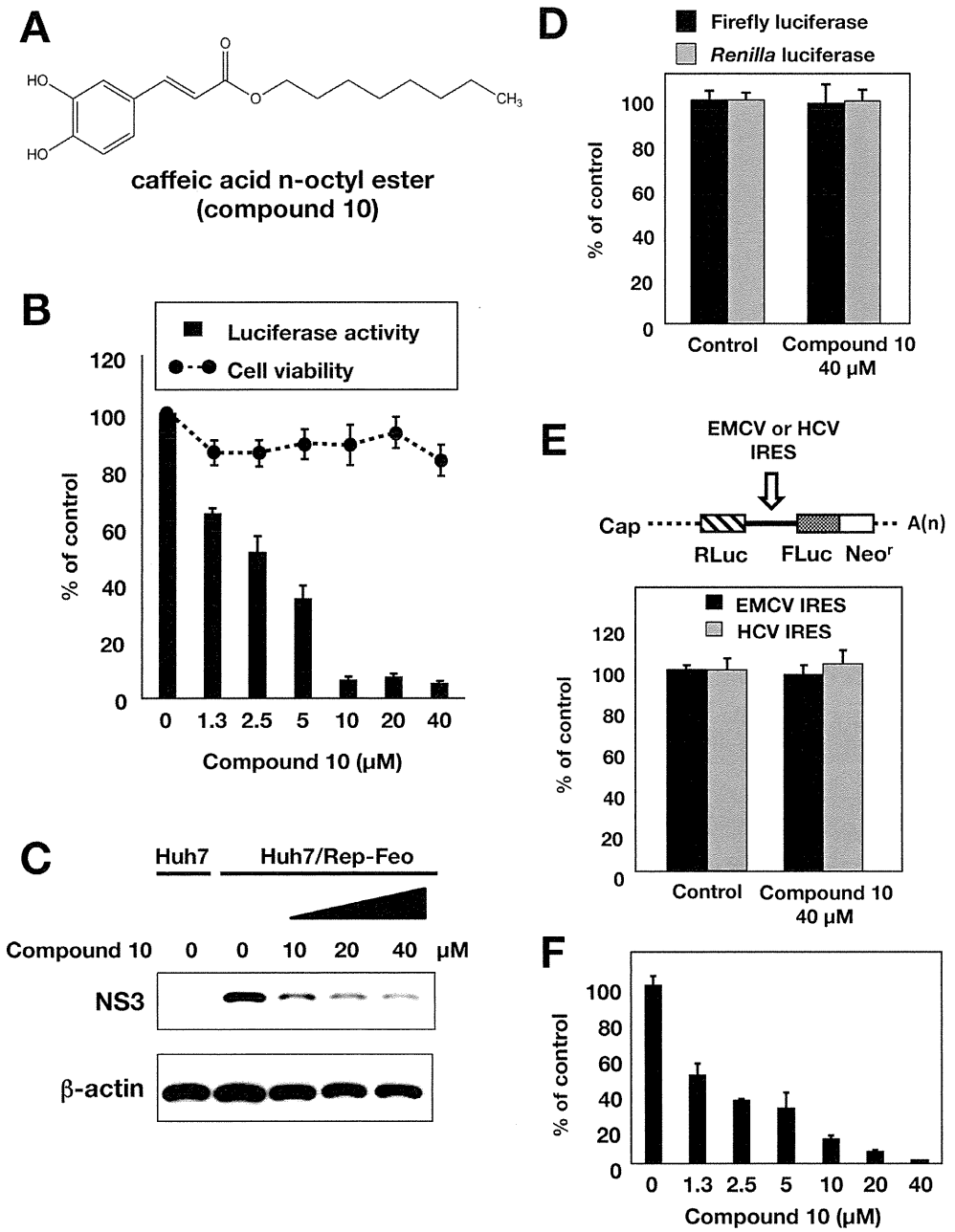

Figure 3. Effect of compound 10 on the viral replication in the replicon cell line and HCVcc. (A) Molecular structure of compound **10**. (B) Huh7/Rep-Feo cells were incubated for 72 h in a medium containing various concentrations of compound **10**. Luciferase and cytotoxicity assays were carried out by the method described in Materials and Methods. Error bars indicate standard deviation. The data represent three independent experiments. (C) Protein extract was prepared from Huh7/Rep-Feo cells treated for 72 h with the indicated concentration of compound **10** and it was then subjected to Western blotting using antibodies to NS3 and beta-actin. (D) Huh7 cell line was transfected with pEF Fluc IN encoding firefly luciferase or pEF Rluc IN encoding *Renilla* luciferase. Both transfected cell lines were incubated with DMSO (Control) or 40 μg/ml compound **10**. Firefly or *Renilla* luciferase activity was measured 72 h post-treatment. Luciferase activity was normalized with protein concentration. Error bars indicate standard deviation. The data were represented from three independent experiments. (E) Schematic structure of RNA transcribed from the plasmids was shown (Top). The bicistronic gene is transcribed under the control of elongation factor 1α (EF1α) promoter. The upstream cistron encoding *Renilla* luciferase (RLuc) is translated by a cap-dependent mechanism. The downstream cistron encodes the fusion protein (Feo), which consists of the firefly luciferase (Fluc) and neomycin phosphotransferase (Neo^r), and is translated under the control of the EMCV or HCV IRES. Huh7 cell line was transfected with each plasmid and incubated for 72 h post-treatment with DMSO (control) or 40 μg/ml of compound **10**. Firefly and *Renilla* luciferase activities were measured. Relative ratio of Firefly luciferase activity to *Renilla* luciferase activity was represented as percentage of the control condition. Error bars indicate standard deviation. The data were represented from three independent experiments. (F) Huh7 OK1 cell line was infected with HCVcc derived from JFH-1 strain and then treated with several concentrations of compound **10** at 24 h post-infection. The resulting cells were harvested 72 h post-infection. The viral RNA of supernatant was purified and estimated by the method described in Materials and Methods. Error bars indicate standard deviation. The data represent three independent experiments. Treatment with DMSO corresponds to '0'.
doi:10.1371/journal.pone.0082299.g003

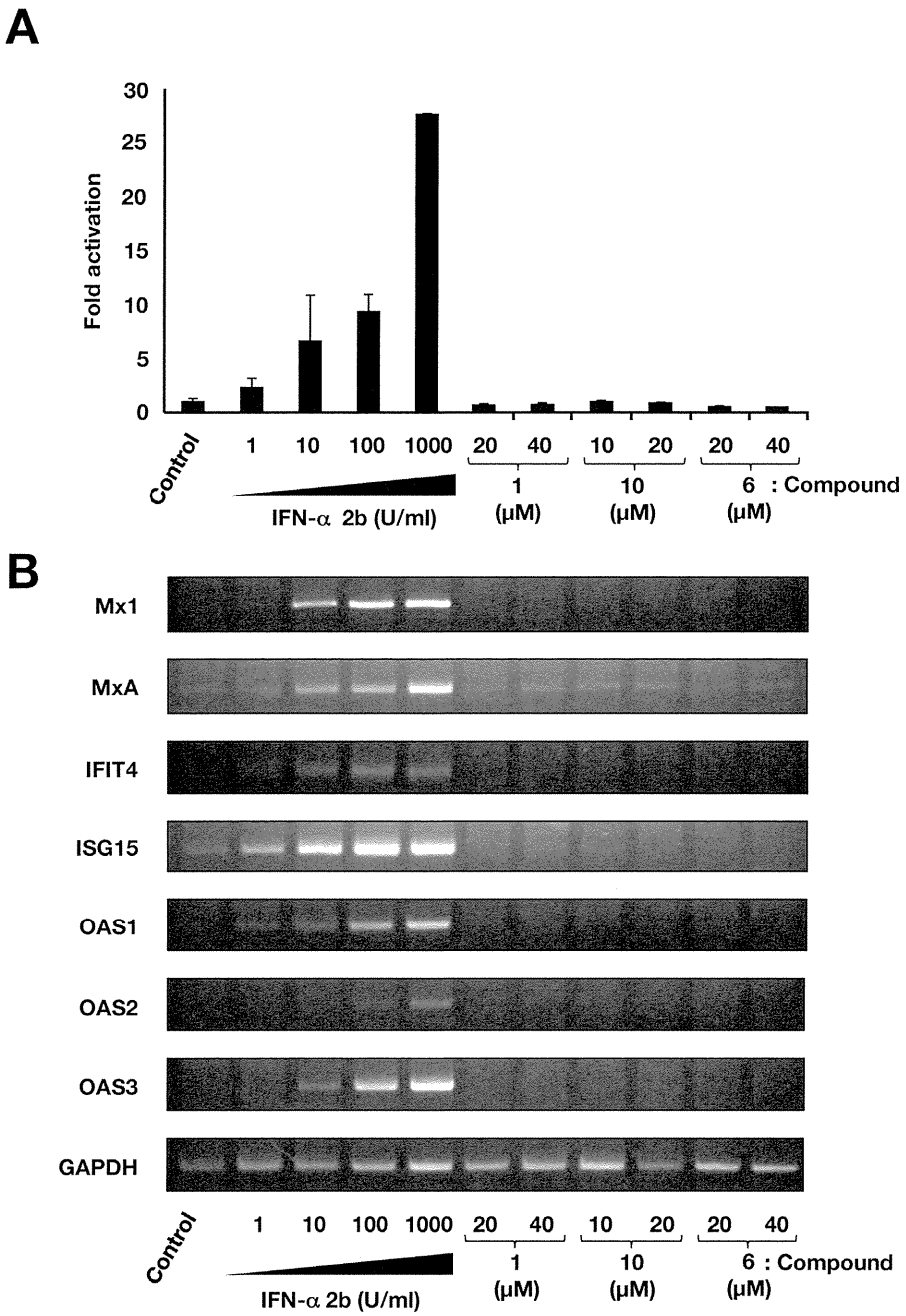

Figure 4. Effect of CAPE derivatives on the interferon-signaling pathway. (A) Plasmids pISRE-TA-Luc and phRG-TK were co-transfect into Huh7 OK1 cells. The transfected cells were cultured with 1, 10, 100, or 1000 U/mL of interferon-alpha 2b, and compounds **1**, **6** and **10**. Treatment with DMSO corresponds to '0'. After 48 h of treatment, luciferase activities were measured, and the value were normalized against *Renilla* luciferase activities. Error bars indicate standard deviation. The data represent three independent experiments. (B) Huh7 replicon cell line of genotype 1b was treated with 1, 10, 100, or 1000 U/mL of interferon-alpha 2b, and compounds **1**, **6** and **10** for 48 h. Treatment with DMSO corresponds to the control. The mRNAs of Mx1, MxA, IFIT4, ISG15, OAS1, OAS2, OAS3, and GAPDH as an internal control were detected by RT-PCR.
doi:10.1371/journal.pone.0082299.g004

of combination tests suggest that daclatasvir, IFN-alpha 2b, and VX-222 synergistically, but telaprevir and danoprevir antagonistically, inhibit HCV replication in combination with compound **10**.

Discussion

CAPE is an active component of propolis, which possesses broad-spectrum biological activities [14–19]. In this study, CAPE suppressed HCV RNA replication in a dose-dependent manner (Fig. 1A and B). Treatment with CAPE inhibited HCV replication with an EC_{50} of 9.0 μM and an SI of 17.9 in Huh7/Rep-Feo cells (Table 1). The treatment of the replicon cell line with CAPE did not induce expression of the IFN-inducible gene (Fig. 4), suggesting that the inhibition of HCV replication by CAPE is independent of the IFN signaling pathway.

Table 5. Anti-HCV activity of compound **10** in replicon cell lines of genotypes 1b and 2a.

Cell line	Replicon type	Strain (Genotype)	EC_{50} [a] (μM)	CC_{50} [b] (μM)	SI [c]
Huh7 Rep/Feo-1b	Subgenome	N (1b)	2.7±0.1	71.7±8.5	26.6
Con1 LUN Sb #26	Subgenome	Con1 (1b)	1.0±0.1	63.1±3.1	63.1
Huh7 Rep/Reo-2a	Subgenome	JFH1 (2a)	1.0±0.3	60.0±2.3	60.0
OR6	Full genome	O (1b)	1.5±0.4	61.7±0.6	41.1

a: Fifty percent effective concentration based on the inhibition of HCV replication.
b: Fifty percent cytotoxicity concentration based on the inhibition of HCV replication.
c: Selectivity Index (CC_{50}/EC_{50}).
doi:10.1371/journal.pone.0082299.t005

We also examined the effect of CAPE derivatives on HCV replication. Our data suggest that the n-alkyl side chain and catechol moiety of the CAPE derivative are critical in its anti-HCV activity (Tables 2 and 3). The EC_{50} value of the derivative decreased dependently on the length of the n-alkyl side chain until reaching octyl ester length (Table 2), while longer chains than octyl ester of a derivative led to an increase in the EC_{50} value and *Clog P* value. Compound **10**, Caffeic acid n-octyl ester, exhibited the highest anti-HCV activity among the tested compounds with an EC_{50} value of 2.7 μM and an SI value of 26.6. Cyclosporine A and its analogues could suppress the viral replication of genotype 1b at a higher level than that of genotype 2a [23]. Interestingly, compound **10** could inhibit HCV replication of genotype 1b and 2a at a similar level, irrespective of expression of the interferon-inducible gene (Fig. 4). CAPE and its derivatives may therefore possess a mechanism different from cyclosporine A and its analogues with respect to anti-HCV activity.

CAPE has been reported to be an inhibitor of NF-kappaB [14,20]. Lee et al. reported that the catechol moiety in CAPE was important for inhibition of NF-kappaB activation [24]. The data shown in Table 3 suggest that the catechol moiety in CAPE is critical to the anti-HCV activity of compound **10**. Previous studies have implicated the inhibition of NF-kappaB in anti-HCV activity. Treatment with an extract prepared from *Acacia confusa* [25] or San-Huang-Xie-Xin-Tang [26] could suppress HCV replication and inhibit NF-kappaB activation. However, Chen et al. reported that curcumin-mediated inhibition of NF-kappaB did not contribute to anti-HCV activity [11]. Furthermore, treatment with *N*′-(Morpholine-4carbonyloxy)-2(naphthalene-1-yl) acetimidamide could activate NF-kappaB and downstream gene expression in the same Huh7/Rep-Feo replicon cell line as the cell line used in this study and exhibited potent inhibition of HCV replication without interferon signaling [27]. These reports support the notion that CAPE derivatives do not mainly target NF-kappaB activity as part of their anti-HCV activity.

Several host proteins have been reported to regulate function of NS5A, leading to supporting HCV replication (review in [2,28]). Daclatasvir exhibited potent synergistic effect on anti-HCV activity in combination of compound **10** (Fig. 5). Anti-HCV activity of compound **10** might associate with intrinsic functions of host factors that interact with NS5A. NS3 protease inhibitors exhibited antagonistic effect in combination of compound **10** (Fig. 5). The inhibitory effect of compound **10** might be mediated by the activation of an unknown endogenous protease that is nonspecifically suppressed by NS3 protease inhibitors. Further study to clarify the mechanism by which compound **10** suppresses HCV replication might contribute to identification of a novel host factor as a drug target for development of the effective compound supporting an effect of other anti-HCV drugs.

In conclusion, we showed that CAPE and its analogue possess a significant inhibitory effect against HCV replication. The length of n-alkyl side chains and the catechol moiety of CAPE are critical to its inhibitory activity against HCV replication. The most effective derivative among the tested compounds was caffeic acid n-octyl ester, which exhibited an EC_{50} value of 1 μM and an SI value of 63.1 in the replicon cell line of genotype 1b strain Con1. Treatment with caffeic acid n-octyl ester reduced the viral replication of genotype 1b and 2a at a similar level and inhibited viral production of HCVcc. Treatment with caffeic acid n-octyl ester could synergistically enhance the anti-HCV activities of IFN-α 2b, daclatasvir, and VX-222, but neither telaprevir nor danoprevir. Further investigation to clarify the mechanism of anti-HCV activity and further modification of the compound to improve anti-HCV activity will lead to novel therapeutic strategies to treat chronic hepatitis C virus infection.

Materials and Methods

Compounds

Boldface numbers in this text indicate the compound numbers shown in Tables. All chemical structures of compounds used in this study are shown in figure S1. CAPE (**1**), caffeic acid (**2**), ferulic acid (**3**), and chlorogenic acid (**5**) and were purchased from Sigma-Aldrich (St. Louis, MO, USA). Cinnamic acid phenethyl ester (**4**) was from Tokyo Chemical Industry (Tokyo, Japan). Rosmarinic acid (**6**) was from Wako Pure Chemical (Tokyo, Japan). Caffeic acid n-octyl ester (n-octyl caffeate) (**10**), 3-O-methylcaffeic acid n-octyl ester (n-octyl-3-methylcaffeate) (**13**), 4-O-methylcaffeic acid n-octyl ester (n-octyl-3-methylcaffeate) (**14**), and 3, 4-O-dimethyl-caffeic acid n-octyl ester (n-octyl-3, 4-methylcaffeate) (**15**) were from LKT Laboratories (St. Paul, MN, USA).

Caffeic acid esters **7**, **8**, **9**, and **11** were synthesized by preparing caffeic acid chloride followed by treatment with corresponding alcohols [29]. Dihydrocaffeic acid ester **12** was prepared by hydrogenation of **7**. Compound **16** is a newly synthesized ester. Spectroscopic data of known esters **7–9**, and **11** prepared here were identical to those reported [30-32] Interferon alfa-2b (IFN-α 2b) was obtained from MSD (Tokyo, Japan). Telaprevir and daclatasvir were purchased from Selleckchem (Houston, TX, USA). Danoprevir and VX-222 were from AdooQ BioScience (Irvine, CA, USA).

Chemistry of 3,4,5-Trihydroxycinnamic acid n-octyl ester

3,4,5-Trihydroxycinnamic acid n-octyl ester (**16**) was prepared by condensation of corresponding benzaldehydes with malonic acid n-octyl monoester [33]. A solution of malonic acid n-octyl monoester (432 mg, 2 mmol), 3,4,5-trihydroxybenzaldehyde (462 mg, 3 mmol) and piperidine (0.2 mL) in pyridine (2 mL)

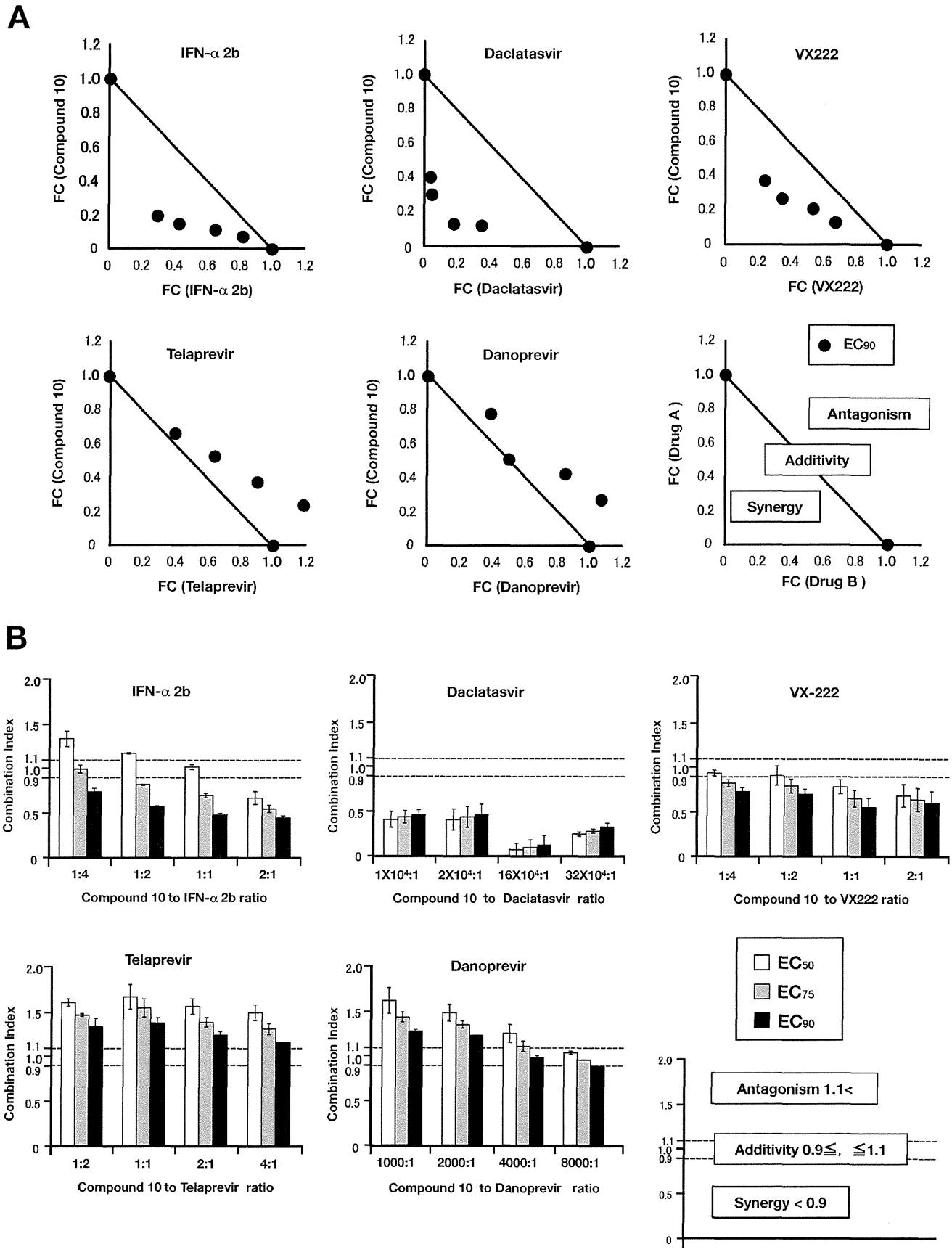
A
IFN-α 2b
FC (Compound 10)
FC (IFN-α 2b)
Daclatasvir
FC (Daclatasvir)
VX222
FC (VX222)
Telaprevir
FC (Telaprevir)
Danoprevir
FC (Danoprevir)
EC90
Antagonism
Additivity
Synergy
FC (Drug A)
FC (Drug B)
B
IFN-α 2b
Combination Index
Compound 10 to IFN-α 2b ratio
Daclatasvir
1X10⁴:1
2X10⁴:1
16X10⁴:1
32X10⁴:1
Compound 10 to Daclatasvir ratio
VX-222
Compound 10 to VX222 ratio
Telaprevir
Compound 10 to Telaprevir ratio
Danoprevir
1000:1
2000:1
4000:1
8000:1
Compound 10 to Danoprevir ratio
EC50
EC75
EC90
Antagonism 1.1<
Additivity 0.9≦, ≦1.1
Synergy < 0.9

Figure 5. Synergistic effect analyses for the combination of compound 10 with IFN-α 2b, daclatasvir, VX-222, telaprevir, or danoprevir. The Huh7 cell line, including the subgenomic replicon RNA of genotype 1b strain Con1, was treated for 72h with combinations of compound 10 and IFN-α 2b, daclatasvir, VX-222, telaprevir, or danoprevir. Luciferase assay were carried out as described in Materials and Methods. (A) The calculated EC_{90} values for combination were plotted as the fractional concentration (FC) of compound 10 and one of IFN-α 2b, daclatasvir, VX-222, telaprevir, and danoprevir on the *x* and *y* axes, respectively. Synergy, antagonism and additivity are indicated in a representative graph as a right end of lower graphs and are described in Materials and Methods. (B) Combination indexes of compound 10 with IFN-α 2b, daclatasvir, VX-222, telaprevir, or danoprevir at the EC50, EC75, and EC90 values were measured at various drug rations. Synergy, antagonism and additivity are indicated in a representative graph as a right end of lower graphs and are described in Materials and Methods.
doi:10.1371/journal.pone.0082299.g005

was heated at 70°C for 1 h. The reaction mixture was concentrated under a vacuum to give a residue, which was dissolved in $CHCl_3$-IPA (3:1, v/v) and then washed with 10% HCl and water. The organic layer was dried over Na_2SO_4 and evaporated to give a residue, which was purified by silica gel column chromatography using AcOEt-hexane (1:1, v/v) as eluent to give the corresponding n-octyl ester (85 mg, 13.8%) as a pale powder. FT-IR vmax (KBr): 3389, 3239, 2923, 1675, 1627, 1606 cm^{-1}. ^1H NMR (400MHz, CD_3OD) δ: 0.86 (3H, t, J= 7.2 Hz), 1.20–1.40 (10H, m), 1.65 (2H, quintet, J= 6.4 Hz), 4.11, (2H, t, J= 6.4 Hz), 6.16 (2H, d, J= 15.6 Hz), 6.55 (2H, s), 7.40 (2H, d, J= 15.6 Hz). 13C NMR (100 Hz, CD_3OD) δ: 14.4, 23.7, 27.1, 29.8, 30.3, 30.4, 32.9, 65.6, 108.5, 115.3, 126.6, 137.5, 147.1, 169.4. CI MS *m/z*: 309 (M^++H). High-resolution CI MS calcd. for $C_{17}H_{25}O_5$ (M^++H) for 309.1702. Found: 309.1686.

Replicon cell lines and virus infection

The Huh7/Rep-Feo cell line, which harbors the subgenomic replicon RNA composed of HCV IRES, the gene of the fusion protein consisting of neomycin phosphotransferase and firefly luciferase, EMCV IRES and a nonstructural gene of genotype 1b strain N in order in Huh7 cell line, was previously established [34]. Thus, the luciferase activity corresponds to the level of HCV RNA replication. The cell line was maintained in Dulbecco's modified Eagle medium containing 10% fetal calf serum and 0.5 mg/mL G418 and cultured in absence of G418 when they were treated with compounds. The Lunet/Con1LUN Sb #26 cell line, which harbors the subgenomic replicon RNA of the Con1 strain (genotype 1b), was described previously [35]. The OR6 cell line, which harbors the full genomic replicon RNA of the O strain (genotype 1b), was described previously [36]. The HCV replicon cell line derived from the genotype 2a strain JFH1 was described previously [37]. The viral RNA derived from the plasmid pJFH1 was transcribed and introduced into Huh7OK1 cells according to the method of Wakita et al. [38]. The virus was amplified by the several times passages. The cells were infected with the virus at a multiplicity of infection (moi) of 1 and then treated with each compound at 24 h post-infection. The culture supernatants were harvested 72 h post-treatment to estimate the viral RNA as described below.

Determination of luciferase activity in HCV replicon cells

The replicon cells were seeded at 2×10^4 cells per well in a 48-well plate 24 h before treatment. Compounds were added to the culture medium to give various concentrations. The resulting cells were harvested 72 h post-treatment and lysed with cell culture lysis reagent (Promega, Madison, WI). The luciferase activity of each cell lysate was estimated using a luciferase assay system (Promega). The resulting luminescence was detected by a Luminescencer-JNR AB-2100 (ATTO, Tokyo, Japan).

Determination of Cytotoxicity in HCV replicon cells

The replicon cells were seeded at a density of 1×10^4 cells per well in a 96-well plate and then incubated at 37°C for 24 h. Compounds were added to the culture medium to give various concentrations and were then harvested 72 h post-treatment. Cell viability was measured using a dimethylthiazol carboxymethoxyphenylsulfophenyl tetrazolium (MTS) assay with a CellTiter 96 aqueous one-solution cell proliferation assay kit (Promega).

Western Blotting

Western blotting was carried out by the method described previously [39]. The antibodies to NS3 (clone 8G-2, mousemonoclonal, Abcam, Cambridge, UK), and beta-actin were purchased from Cell Signaling Technology (rabbit polyclonal, Danvers, MA, USA) and were used as the primary antibodies in this study.

RNA analysis

Total RNAs were prepared from cells by using the RNAqueous-4PCR kit (Life Technologies, Carlsbad, CA). Viral RNA were prepared from culture supernatants by using the QIAamp Viral RNA mini kit (QIAGEN, Hilden, Germany). The viral RNA genome was estimated by the qRT-PCR method described previously [40]. RT-PCR was carried out by the method described previously [41] which was slightly modified at the PCR step. The PCR samples were incubated once for 10 min at 95°C for an initial activation step of the AmpliTaq Gold DNA Polymerase (Life Technologies), and then subjected to an amplification step of 30 repeats of the cycle consisting of three segments as follow: 0.5 min at 95°C, 1 min at 55°C and 1 min at 72°C. The primers used in this study were as follows: Mx1: 5′-AGCCACTGGACTGACGACTT-3′ and 5′-GAGGGCTGAAAATCCCTTTC-3′;

MxA: 5′-GTCAGGAGTTGCCCTTCCCA-3′ and 5′-ATTCCCATTCCTTCCCCGG-3′;

IFIT4: 5′-CCCTTCAGGCATAGGCAGTA-3′ and 5′-CTCCTACCCGTCACAACCAC -3′; ISG15: 5′-CGCAGATCACCCAGAAGAT-3′ and 5′-GCCCTTGTTATTCCTCACCA-3′;

OAS1: 5′-CAAGCTCAAGAGCCTCATCC-3′ and 5′-TGGGCTGTGTTGAAATGTGT-3′;

OAS2: 5′-ACAGCTGAAAGCCTTTTGGA-3′ and 5′-GCATTAAAGGCAGGAAGCAC-3′;

OAS3: 5′-CACTGACATCCCAGACGATG-3′ and 5′-GATCAGGCTCTTCAGCTTGGC-3′;

GAPDH: 5′-GAAGGTGAAGGTCGGAGTC and 5′- GAAGATGGTGATGGGATTTC-3′

Effects on activities of internal ribosome entry site (IRES) and luciferases

Huh7 OK1 cells were transfected with pEF.Rluc.HCV.IRES.-Feo or pEF.Rluc.EMCV.IRES.Feo [39]. These transfected cells were seeded at 2×10^4 cells per well in a 48-well plate 24 h before treatment, treated with DMSO or compound **10**, and then harvested at 72 h post-treatment. The firefly luciferase activities were measured with a luciferase assay system (Promega). The total protein concentration was measured using the BCA Protein Assay Reagent Kit (Thermo Scientific, Rockford, IL, USA) to normalize

luciferase activity. To evaluate the interferon response, Huh7OK1 cells were seeded on a 48 well plate at a density of 2×10^4 cells per well, and transfected with pISRE-TA-Luc (Takara bio, Shiga, Japan) and phRG-TK (Promega). These transfected cells were incubated in the presence of compounds, IFN-α 2b, or DMSO, and then harvested at 48 h post-treatment. The firefly luciferase and *Renilla* luciferase activities were quantified by using Dual luciferase reporter assay system (Promega).

Prediction of Clog*P* for compounds

The *C*log*P* value deduced from chemical structure roughly corresponds to a value of hydrophobicity. The *C*log*P* values of compounds used in this study were calculated using the computer software Chem Bio Office Ultra 2008 (PerkinElmer, Cambridge, MA, USA).

Synergistic effect of caffeic acid n-octyl ester on anti-HCV activities of other drugs

The effects of drug-drug combinations were evaluated by using the Con1 LUN Sb #26 replicon cells, and were analyzed by using the computer software CalcuSyn (Biosoft, Cambridge, United Kingdom). Dose inhibition curves of two different drugs were plotted with each other. In each drug combination, EC_{90} values of several combinations of two different drugs were plotted as the fractional concentration (FC) of both drugs on the x and y-axes. Additivity indicates the line linked between 1.0 FC value points of both drugs in the absence of each other. Synergy and antagonism are indicated by values plotted under and above, respectively, an additivity line. The explanatory diagram of isobologram is shown in a right end of lower panels of Figure 5A. Combination indexes (CIs) were calculated at the EC_{50}, EC_{75}, and EC_{90} by using CalcuSyn. A CI value of less than 0.9 indicates synergy. A CI value ranging from 0.9 to 1.1 indicates additivity. A CI value of more than 1.1 indicates antagonism. The explanatory diagram was shown in a right end of lower panels of Figure 5B.

Supporting Information

Figure S1 Molecular structure of CAPE and commercial CAPE-related compounds. CAPE structure is divided into three parts: (I) the catechol moiety, (II) the alkenyl moiety on alpha, beta -unsaturated ester, and (III) the ester part. Molecular structures of CAPE and its commercial derivatives are shown.
(TIF)

Figure S2 The basic structure and side moieties of compounds shown in Table 2. Each compound structure is represented on the basis of the basic structure (top).
(TIF)

Figure S3 The molecular structures of compounds 7 and 12, which are shown in Table 3. Both compounds are different in alpha, beta-unsaturated or saturated part attached to ester.
(TIF)

Figure S4 The basic structure and side moieties of compounds shown in Table 4. Each compound structure is represented on the basis of the basic structure (top).
(TIF)

Acknowledgments

We thank T. Wakita for kindly providing a plasmid.

Author Contributions

Conceived and designed the experiments: MT KM. Performed the experiments: H. Shen AY MN HY MS H. Shindo SM. Analyzed the data: HK TT NE. Contributed reagents/materials/analysis tools: YF MI NK NS. Wrote the paper: H. Shen AY MT KM.

References

1. Baldo V, Baldovin T, Trivello R, Floreani A (2008) Epidemiology of HCV infection. Curr Pharm Des 14: 1646–1654.
2. Moriishi K, Matsuura Y (2012) Exploitation of lipid components by viral and host proteins for hepatitis C virus infection. Front Microbiol 3: 54.
3. Hijikata M, Kato N, Ootsuyama Y, Nakagawa M, Shimotohno K (1991) Gene mapping of the putative structural region of the hepatitis C virus genome by in vitro processing analysis. Proc Natl Acad Sci USA 88: 5547–5551.
4. Lohmann V, Korner F, Koch J, Herian U, Theilmann L, et al. (1999) Replication of subgenomic hepatitis C virus RNAs in a hepatoma cell line. Science 285: 110–113.
5. Hofmann WP, Zeuzem S (2011) A new standard of care for the treatment of chronic HCV infection. Nat Rev Gastroenterol Hepatol 8: 257–264.
6. Jacobson IM, McHutchison JG, Dusheiko G, Di Bisceglie AM, Reddy KR, et al. (2011) Telaprevir for previously untreated chronic hepatitis C virus infection. N Engl J Med 364: 2405–2416.
7. Sarrazin C, Hezode C, Zeuzem S, Pawlotsky JM (2012) Antiviral strategies in hepatitis C virus infection. J Hepatol 56 Suppl 1: S88–100.
8. Kieffer TL, Kwong AD, Picchio GR (2010) Viral resistance to specifically targeted antiviral therapies for hepatitis C (STAT-Cs). J Antimicrob Chemother 65: 202–212.
9. Ahmed-Belkacem A, Ahnou N, Barbotte L, Wychowski C, Pallier C, et al. (2010) Silibinin and related compounds are direct inhibitors of hepatitis C virus RNA-dependent RNA polymerase. Gastroenterology 138: 1112–1122.
10. Calland N, Albecka A, Belouzard S, Wychowski C, Duverlie G, et al. (2012) (-)-Epigallocatechin-3-gallate is a new inhibitor of hepatitis C virus entry. Hepatology 55: 720–729.
11. Chen MH, Lee MY, Chuang JJ, Li YZ, Ning ST, et al. (2012) Curcumin inhibits HCV replication by induction of heme oxygenase-1 and suppression of AKT. Int J Mol Med 30: 1021–1028.
12. Bachmetov L, Gal-Tanamy M, Shapira A, Vorobeychik M, Giterman-Galam T, et al. (2012) Suppression of hepatitis C virus by the flavonoid quercetin is mediated by inhibition of NS3 protease activity. J Viral Hepat 19: e81–88.
13. Takeshita M, Ishida Y, Akamatsu E, Ohmori Y, Sudoh M, et al. (2009) Proanthocyanidin from blueberry leaves suppresses expression of subgenomic hepatitis C virus RNA. J Biol Chem 284: 21165–21176.
14. Toyoda T, Tsukamoto T, Takasu S, Shi L, Hirano N, et al. (2009) Anti-inflammatory effects of caffeic acid phenethyl ester (CAPE), a nuclear factor-kappaB inhibitor, on Helicobacter pylori-induced gastritis in Mongolian gerbils. Int J Cancer 125: 1786–1795.
15. Ho CC, Lin SS, Chou MY, Chen FL, Hu CC, et al. (2005) Effects of CAPE-like compounds on HIV replication in vitro and modulation of cytokines in vivo. J Antimicrob Chemother 56: 372–379.
16. Chiao C, Carothers AM, Grunberger D, Solomon G, Preston GA, et al. (1995) Apoptosis and altered redox state induced by caffeic acid phenethyl ester (CAPE) in transformed rat fibroblast cells. Cancer Res 55: 3576–3583.
17. Boudreau LH, Maillet J, LeBlanc LM, Jean-Francois J, Touaibia M, et al. (2012) Caffeic acid phenethyl ester and its amide analogue are potent inhibitors of leukotriene biosynthesis in human polymorphonuclear leukocytes. PLoS One 7: e31833.
18. Lee KW, Chun KS, Lee JS, Kang KS, Surh YJ, et al. (2004) Inhibition of cyclooxygenase-2 expression and restoration of gap junction intercellular communication in H-ras-transformed rat liver epithelial cells by caffeic acid phenethyl ester. Ann N Y Acad Sci 1030: 501–507.
19. Fesen MR, Kohn KW, Leteurtre F, Pommier Y (1993) Inhibitors of human immunodeficiency virus integrase. Proc Natl Acad Sci U S A 90: 2399–2403.
20. Natarajan K, Singh S, Burke TR Jr, Grunberger D, Aggarwal BB (1996) Caffeic acid phenethyl ester is a potent and specific inhibitor of activation of nuclear transcription factor NF-kappa B. Proc Natl Acad Sci U S A 93: 9090–9095.
21. Li Y, Zhang T, Douglas SD, Lai JP, Xiao WD, et al. (2003) Morphine enhances hepatitis C virus (HCV) replicon expression. Am J Pathol 163: 1167–1175.
22. Okamoto T, Omori H, Kaname Y, Abe T, Nishimura Y, et al. (2008) A single-amino-acid mutation in hepatitis C virus NS5A disrupting FKBP8 interaction impairs viral replication. J Virol 82: 3480–3489.
23. Ishii N, Watashi K, Hishiki T, Goto K, Inoue D, et al. (2006) Diverse effects of cyclosporine on hepatitis C virus strain replication. J Virol 80: 4510–4520.

24. Lee Y, Shin DH, Kim JH, Hong S, Choi D, et al. (2010) Caffeic acid phenethyl ester-mediated Nrf2 activation and IkappaB kinase inhibition are involved in NFkappaB inhibitory effect: structural analysis for NFkappaB inhibition. Eur J Pharmacol 643: 21–28.
25. Lee JC, Chen WC, Wu SF, Tseng CK, Chiou CY, et al. (2011) Anti-hepatitis C virus activity of Acacia confusa extract via suppressing cyclooxygenase-2. Antiviral Res 89: 35–42.
26. Lee JC, Tseng CK, Wu SF, Chang FR, Chiu CC, et al. (2011) San-Huang-Xie-Xin-Tang extract suppresses hepatitis C virus replication and virus-induced cyclooxygenase-2 expression. J Viral Hepat 18: e315–324.
27. Kusano-Kitazume A, Sakamoto N, Okuno Y, Sekine-Osajima Y, Nakagawa M, et al. (2012) Identification of novel N-(morpholine-4-carbonyloxy) amidine compounds as potent inhibitors against hepatitis C virus replication. Antimicrob Agents Chemother 56: 1315–1323.
28. Moradpour D, Penin F, Rice CM (2007) Replication of hepatitis C virus. Nat Rev Microbiol 5: 453–463.
29. Lee YJ, Liao PH, Chen WK, Yang CY (2000) Preferential cytotoxicity of caffeic acid phenethyl ester analogues on oral cancer cells. Cancer Lett 153: 51–56.
30. Bourne GT, Golding SW, McGeary RP, Meutermans WD, Jones A, et al. (2001) The development and application of a novel safety-catch linker for BOC-based assembly of libraries of cyclic peptides. J Org Chem 66: 7706–7713.
31. Nagaoka T, Banskota AH, Tezuka Y, Saiki I, Kadota S (2002) Selective antiproliferative activity of caffeic acid phenethyl ester analogues on highly liver-metastatic murine colon 26-L5 carcinoma cell line. Bioorg Med Chem 10: 3351–3359.
32. Uwai K, Osanai Y, Imaizumi T, Kanno S, Takeshita M, et al. (2008) Inhibitory effect of the alkyl side chain of caffeic acid analogues on lipopolysaccharide-induced nitric oxide production in RAW264.7 macrophages. Bioorg Med Chem 16: 7795–7803.
33. Zhang Z, Xiao B, Chen Q, Lian XY (2010) Synthesis and biological evaluation of caffeic acid 3,4-dihydroxyphenethyl ester. J Nat Prod 73: 252–254.
34. Yokota T, Sakamoto N, Enomoto N, Tanabe Y, Miyagishi M, et al. (2003) Inhibition of intracellular hepatitis C virus replication by synthetic and vector-derived small interfering RNAs. EMBO Rep 4: 602–608.
35. Frese M, Barth K, Kaul A, Lohmann V, Schwarzle V, et al. (2003) Hepatitis C virus RNA replication is resistant to tumour necrosis factor-alpha. Journal of General Virology 84: 1253–1259.
36. Ikeda M, Abe K, Dansako H, Nakamura T, Naka K, et al. (2005) Efficient replication of a full-length hepatitis C virus genome, strain O, in cell culture, and development of a luciferase reporter system. Biochem Biophys Res Commun 329: 1350–1359.
37. Nishimura-Sakurai Y, Sakamoto N, Mogushi K, Nagaie S, Nakagawa M, et al. (2010) Comparison of HCV-associated gene expression and cell signaling pathways in cells with or without HCV replicon and in replicon-cured cells. J Gastroenterol 45: 523–536.
38. Wakita T, Pietschmann T, Kato T, Date T, Miyamoto M, et al. (2005) Production of infectious hepatitis C virus in tissue culture from a cloned viral genome. Nat Med 11: 791–796.
39. Yamashita A, Salam KA, Furuta A, Matsuda Y, Fujita O, et al. (2012) Inhibition of hepatitis C virus replication and NS3 helicase by the extract of the feather star *Alloeocomatella polycladia*. Mar Drugs 10: 744–761.
40. Fujimoto Y, Salam KA, Furuta A, Matsuda Y, Fujita O, et al. (2012) Inhibition of Both Protease and Helicase Activities of Hepatitis C Virus NS3 by an Ethyl Acetate Extract of Marine Sponge Amphimedon sp. PLoS One 7: e48685.
41. Jin H, Yamashita A, Maekawa S, Yang PT, He LM, et al. (2008) Griseofulvin, an oral antifungal agent, suppresses hepatitis C virus replication in vitro. Hepatology Research 38: 909–918.

J Gastroenterol (2014) 49:163–164
DOI 10.1007/s00535-013-0926-7

EDITORIAL

Once-daily simeprevir in combination with pegylated-interferon and ribavirin: a new horizon in the era of direct-acting antiviral agent therapy for chronic hepatitis C

Shinya Maekawa · Nobuyuki Enomoto

Received: 7 December 2013 / Accepted: 10 December 2013 / Published online: 21 December 2013

Hepatitis C virus (HCV) is a leading cause of chronic hepatitis, liver cirrhosis, and hepatocellular carcinoma (HCC), and it is estimated that infected individuals total 185 million people worldwide. In Japan, around 2 million are infected with HCV, and more than 20 thousand die from HCV-induced HCC annually. Though viral eradication with antiviral therapies is the most important and effective choice for decreasing HCC-related deaths induced by HCV, complete viral eradication has been quite difficult till recently, especially in patients with genotype-1 HCV infection because of the low response rate to interferon (IFN)-based therapy [1, 2].

In this background, development of novel direct-acting antiviral agents (DAAs) specific for HCV was truly a revolutionary event. In 2011, two first-generation NS3 protease inhibitors (PIs), telaprevir and boceprevir, were firstly approved among all the DAAs for clinical use in USA and Europe for genotype-1 HCV in combination with pegylated-interferon and ribavirin (PR), while telaprevir was approved in Japan in the same 2011 period. As expected, a regimen including telaprevir in combination with pegylated-interferon and ribavirin dramatically improved the sustained viral response (SVR) rate to as high as 80 % in genotype-1 HCV infection. On the other hand, telaprevir has several undesirable problems. Among all, adverse events (AEs) of anemia and skin rash are serious problems of telaprevir, and Grade 3/4 skin disorders, including Stevens–Johnson syndrome and drug rashes with eosinophilia and systemic symptoms, as well as Grade 3 anemia (<8.0 g/dL), might occur [3, 4]. Moreover, cumbersome frequent dosing three times a day (every 7–9 h) could induce poor medication adherence. Under the circumstances, it has been quite stressful for patients as well as clinicians to introduce and monitor this telaprevir-based regimen.

Simeprevir (SMV, TMC435) is classified as a second-generation PI with the macrocyclic structure having an advantage in the binding affinity and specificity for NS3 protease compared to the first-generation PI with the linear structure. Due to the difference in the structure, the drug-resistance profile is somewhat different from that of telaprevir. Though simeprevir shows cross-resistance with telaprevir at amino acid positions of 155 and 156, most of the resistant mutation occurs at the simeprevir-specific amino acid position of 168 [5]. Though simeprevir is effective in all viral genotypes (genotype 1–6), it has the strongest antiviral activity for genotype-1a and -1b HCV infection. In particular, low AE rate and its patient-friendly once-daily dosing are the important characters of simeprevir aside from its strong antiviral activity. In the international phase II trials of simeprevir in combination with PegIFNa-2a/RBV for treatment-naïve (PILLAR study) [6] and treatment-experienced patients (ASPIRE study) [7] for HCV genotype 1-infected patients, it was demonstrated that simeprevir was generally well tolerated and had a pharmacokinetic profile supporting once-a-day (QD) dosing resulting in high virologic response rates.

In this issue of the *Journal of Gastroenterology*, Hayashi et al. [8] reported the important results of the phase II *D*ose and duration *R*anging study of *A*ntiviral agent TMC435 in *G*enotype *O*ne HCV treatment-*N*aïve patients (DRAGON study; TMC435-C215) evaluating once-daily simeprevir

This comment refers to the article available at doi:10.1007/s00535-013-0875-1.

S. Maekawa (✉) · N. Enomoto
First Department of Internal Medicine, Faculty of Medicine, University of Yamanashi, 1110 Shimokato, Chuo, Yamanashi 409-3898, Japan
e-mail: maekawa@yamanashi.ac.jp

with pegylated-interferon and ribavirin therapy for treatment-naïve, high viral-loaded hepatitis C genotype 1-infected patients in Japan. Due to the result of previous phase I study that simeprevir plasma concentration was higher in Japanese healthy volunteers compared with Caucasian volunteers, simeprevir doses of 50/100 mg QD were selected for this study, while simeprevir doses of 150 mg QD were selected in western countries [9]. Through investigating five treatment groups (SMV12/PR24 50 mg, SMV12/PR24 100 mg, SMV24/PR24 50 mg, SMV24/PR24 100 mg, and PR48), it was disclosed that simeprevir-combined groups all achieved high SVR rate (77–92 % compared to 46 % for PR). As to the AEs, simeprevir was well tolerated, and the incidence of anemia and skin rash were similar in their frequency and their grade between all the SMV groups and the PR group. Due to low AEs, therapy discontinuation rate and ribavirin dose reduction was also similar in the SMV groups and the PR group. While an AE of bilirubin elevation was specific to simeprevir, and it reached to grade 3 (2.6–5.0 mg/dL) to 4 (>5.0 mg/dL) in four patients (5 %) leading to the discontinuation of simeprevir in these individuals, the bilirubin level returned to baseline after the end of simeprevir in those patients. Since bilirubin elevation is considered to result from the blockade of bilirubin clearance-associated OATP1B1 and MRP transporters by simeprevir [10], it is considered that the bilirubin elevation by simeprevir does not reflect deterioration of liver function.

Following the results of this phase II DRAGON study, treatment dosage of simeprevir was determined as 100 mg QD in Japan, and successive phase III CONCERTO studies for simeprevir/pegylated-interferon/ribavirin therapy have been conducted (CONCERTO-1 for treatment-naïve, -2 for previous null responder, -3 for previous relapser, and -4 for naïve, null responder and relapser). After the completion of those CONCERTO studies with favorable outcomes for simeprevir-based regimens, once-daily simeprevir with pegylated-interferon and ribavirin therapy for high viral-loaded hepatitis C genotype 1-infected patients was just recently approved for clinical use in Japan.

Considering the history of HCV therapy, this new therapy of once-daily simeprevir with pegylated-interferon and ribavirin therapy is ideal in its high efficacy and low AEs. Of course, it is true that DAA combination therapies without IFN (IFN-free therapies) would appear in the near future, and that these IFN-free therapies are advantageous in that they are free from IFN-related AEs. However, in terms of DAA-resistant viral mutants, it is considered that these mutant HCVs generally have low replication fitness, and are sensitive to IFN. Therefore, it is speculated that IFN-based DAA therapies compared to IFN-free DAA therapies are safer in preventing the development of multidrug resistant HCVs.

Taken together, the new regimen of once-daily simeprevir with pegylated-interferon and ribavirin therapy would surely be an important milestone in the therapy for high viral-loaded hepatitis C genotype-1 infected patients in the era of DAA therapy.

References

1. Kim MN, Kim BK, Han KH. Hepatocellular carcinoma in patients with chronic hepatitis C virus infection in the Asia-Pacific region. J Gastroenterol. 2013;48(6):681–8.
2. Thomas DL. Global control of hepatitis C: where challenge meets opportunity. Nat Med. 2013;19(7):850–8.
3. Chayama K, Hayes CN, Ohishi W, Kawakami Y. Treatment of chronic hepatitis C virus infection in Japan: update on therapy and guidelines. J Gastroenterol. 2013;48(1):1–12.
4. Kumada H, Toyota J, Okanoue T, Chayama K, Tsubouchi H, Hayashi N. Telaprevir with peginterferon and ribavirin for treatment-naive patients chronically infected with HCV of genotype 1 in Japan. J Hepatol. 2013;56(1):78–84.
5. Lenz O, Verbinnen T, Lin TI, Vijgen L, Cummings MD, Lindberg J, et al. In vitro resistance profile of the hepatitis C virus NS3/4A protease inhibitor TMC435. Antimicrob Agents Chemother. 2010;54(5):1878–87.
6. Fried MW, Buti M, Dore GJ, Flisiak R, Ferenci P, Jacobson I, et al. Once-daily simeprevir (TMC435) with pegylated interferon and ribavirin in treatment-naive genotype 1 hepatitis C: the randomized PILLAR study. Hepatology. 2013;58(6):1918–29.
7. Zeuzem S, Berg T, Gane E, Ferenci P, Foster GR, Fried MW, et al. Simeprevir increases rate of sustained virologic response among treatment-experienced patients with HCV genotype-1 infection: a phase IIb trial. Gastroenterology. 2013. doi:10.1053/j.gastro.2013.10.058.
8. Hayashi N, Seto C, Kato M, Komada Y, Goto S. Once-daily simeprevir (TMC435) with peginterferon/ribavirin for treatment-naïve hepatitis C genotype 1-infected patients in Japan: the DRAGON study. J Gastroenterol. 2013. doi:10.1007/s00535-013-0875-1.
9. Verloes R, Shishido A. Phase I safety and PK of TMC435 in healthy volunteers and safety, PK and short-term efficacy in chronic hepatitis C infected individuals. Kobe: Abstract O-32 presented at the Japanese Hepatology Congress; 2009. p. 4–5.
10. Huisman MT, Snoeys J, Monbaliu J, Martens M, Sekar V, Raoof A. In vitro studies investigating the mechanism of interaction between TMC435 and hepatic transporters. Poster 278 presented at the 61st Annual Meeting of the American Association for the Study of Liver Diseases (AASLD), Boston, USA, October 29–November 2, 2010.

Original Research

Association of Splenic MR Elastographic Findings With Gastroesophageal Varices in Patients With Chronic Liver Disease

Hiroyuki Morisaka, MD,[1] Utaroh Motosugi, MD, PhD,[1]* Shintaro Ichikawa, MD,[1] Katsuhiro Sano, MD, PhD,[1] Tomoaki Ichikawa, MD, PhD,[1] and Nobuyuki Enomoto, MD, PhD[2]

Purpose: To identify magnetic resonance imaging (MRI)-based parameters associated with gastroesophageal varices (GEVs) in patients with chronic liver disease.

Materials and Methods: Ninety-three patients were divided into three groups based on endoscopic findings: group 1 with no GEVs ($n=49$), group 2 with mild GEVs ($n=30$), and group 3 with severe GEVs ($n=14$). We used a multivariate logistic regression analysis to assess liver stiffness, aspartate aminotransferase-to-platelet ratio index, spleen stiffness and volume, portal vein velocity, cross-sectional area, and flow volumes potential independent associators of any (mild and severe) GEVs or severe GEVs.

Results: The analysis showed that spleen and liver stiffness and spleen volume were independently associated with any GEVs (spleen stiffness, odds ratio [95% confidence interval], 1.25 [1.04–1.68], $P=0.018$; liver stiffness, 1.52 [1.13–2.17], $P=0.006$; spleen volume, 1.01 [1.00–1.01], $P=0.016$), whereas spleen stiffness was associated with severe GEVs (1.82 [1.25–2.95]; $P=0.005$).

Conclusion:: Liver and spleen stiffness and spleen volume are associated with GEVs in patients with chronic liver disease. Compared with liver stiffness and spleen volume, spleen stiffness is more strongly associated with severe GEVs.

Key Words: MR elastography; liver cirrhosis; portal hypertension; spleen stiffness; phase-contrast MRI
J. Magn. Reson. Imaging 2013;00:000–000.

GASTROESOPHAGEAL VARICES (GEVs) and GEV-related bleeding are severe complications of portal hypertension (PH) in cirrhosis (1). Screening is indicated in patients with newly diagnosed cirrhosis, and medical treatment must be considered as soon as varices are detected to prevent the first bleeding (2). Upper endoscopy is the first-line investigation to identify GEVs. The examination itself is not associated with serious complications but, if it has to be repeated during follow-up in cirrhotic patients, it is time-consuming and costly. Therefore, a number of noninvasive imaging and biochemical methods for the assessment of GEVs have been developed. In particular, ultrasound techniques for the measurement of liver stiffness (LS) (3), spleen diameter (4,5), portal vein (PV) flow (6,7), and hepatic venous waveforms (8) as well as for the morphological assessment of the portal venous system (7) have been investigated and validated. Other noninvasive methods using computed tomography and magnetic resonance imaging (MRI) have also been reported (9,10).

Liver fibrosis plays a fundamental role in the development of PH in patients with cirrhosis. Therefore, patients at a high risk of GEVs can be identified using the same parameters as those for evaluating liver fibrosis, including LS (measured by elastography) and blood biochemical indices (eg, the aspartate aminotransferase [AST]-to-platelet ratio index [APRI]) (11). It has been previously shown that LS, measured using ultrasound transient elastography, correlates with the hepatic vein pressure gradient (12).

Splenomegaly also plays an important role in the pathophysiology of PH by increasing splanchnic inflow (13). Recently, spleen stiffness (SS) assessed with ultrasound transient elastography has been shown to be a more effective parameter for evaluating the hepatic vein pressure gradient and GEVs than LS (14,15).

LS can be evaluated by magnetic resonance elastography (MRE), which has been recently shown to have considerably high reproducibility, repeatability, and validity for assessing liver fibrosis (16–19). MRE can also be used to evaluate SS (20). Recent studies with animal models have revealed that SS measured by MRE is well correlated with the hepatic venous

[1]Department of Radiology, University of Yamanashi, Yamanashi, Japan.
[2]1st Department of Internal Medicine, University of Yamanashi, Yamanashi, Japan.
*Address reprint requests to: U.M., Department of Radiology, University of Yamanashi, 1110 Shimokato, Chuo-shi, Yamanashi-ken 409-3898, Japan. E-mail: utaroh-motosugi@nifty.com
Received July 16, 2013; Accepted October 16, 2013.
DOI 10.1002/jmri.24505
View this article online at wileyonlinelibrary.com.

Table 1
Acquisition Parameters for MRE and Phase-Contrast MRI

Parameters	MR elastography	Phase-contrast MRI
Sequence	Gradient echo	Gradient echo
TR/TE (msec)	100/27	12.5/5.0
Flip angle (degrees)	30	20
Slice thickness (mm)	10	10
FOV (cm)	30–34 × 40–45	40 × 28
Matrix	256 × 64	256 × 128
Number of slices	2	1
Other	Frequency of pneumatic driver: 60 Hz Phase offsets: 4	VENC parallel to flow direction: 30 cm/s No. of phases: 32

TR/TE = repetition time/echo time, FOV = field of view, VENC = velocity encoding.

pressure gradient and can be a better predictor of PH than LS (21,22). It is hypothesized that increased PH may directly reflect SS, whereas LS represents both liver fibrosis and portal pressure. As with ultrasound-based portal flow measurement (6,7), another MRI-based approach for evaluating PH and GEVs is phase-contrast MRI (PC-MRI). PV flow measured by PC-MRI was shown to correlate with PH and to be useful in predicting GEVs (23,24).

Thus, the aim of this study was to identify useful MRI parameters that are associated with the severity of GEVs in patients with chronic liver disease (CLD).

MATERIALS AND METHODS

Subjects

This retrospective study was approved by our Institutional Review Board. Between September 2011 and March 2012, 210 patients with CLD (age range, 27–87 years; mean and standard deviation, 68 ± 11 years; male-to-female ratio, 138:82) underwent MRE of the liver and spleen and PC-MRI of the PV in a single MRI examination, which was performed as a routine clinical practice (eg, search for hepatocellular carcinoma). Patients who met at least one of the following criteria were excluded from the study ($n=117$): 1) no upper endoscopic examination within 6 months preceding the MRI examination ($n=86$); 2) a history of interventional treatment for GEVs, including endoscopic ligation ($n=13$) and balloon-occluded retrograde transvenous obliteration ($n=2$) that might have altered the hemodynamics of the portal venous system; 3) failure of MRE image due to high iron deposition ($n=2$ for the liver; $n=2$ for the spleen); 4) failure of PC-MRI due to motion artifacts ($n=7$); 5) presence of a PV thrombus confirmed by contrast-enhanced computed tomography ($n=2$) or a history of partial splenic embolization ($n=1$); or 6) a history of lobectomy or more than one segmentectomy of the liver ($n=2$). After exclusion, the study cohort comprised 93 patients with CLD, all of whom underwent at least one upper endoscopic examination within 6 months of the MRI examination. The mean and standard deviation of the time between MRI and upper endoscopy was 1.4 ± 2.7 months; range, −3.3 to 5.9 months (negative value indicates that MRI was performed followed by upper endoscopy). We included some patients who underwent upper endoscopy after MRI examination because endoscopic examinations were scheduled as a clinical follow-up for the development of GEVs and we were not able to properly coordinate and control the schedule of examination.

The types and distribution of CLD were as follows: hepatitis C virus infection ($n=59$), hepatitis B virus infection ($n=12$), alcoholic liver disease ($n=6$), autoimmune liver disease ($n=3$), and others ($n=13$). Patient characteristics were as follows: age, 69 ± 8 years; body mass index (BMI), 20.8 ± 7 kg/m^2; male-to-female ratio, 59:34; and Child-Pugh classes A ($n=74$), B ($n=17$), and C ($n=2$). Liver tissue samples were available for pathological assessment of liver fibrosis in 36 of 93 patients (31 biopsy and 5 surgically resected samples). Twelve patients had mild bridging fibrosis, 10 had moderate bridging fibrosis, and 14 had cirrhosis.

Reference Standards for GEVs

All upper endoscopic examinations were performed by gastroenterologists who specialized in endoscopy. They recorded the presence or absence of GEVs and, if present, noted their forms and any red-color signs, according to the previously described guidelines (25). GEVs were categorized as straight and small (F1), moderately enlarged and beady (F2), or markedly enlarged with a nodular or tumor-like shape (F3). Patients were divided into three groups according to the types of GEVs and red-color signs: 1) a group with no GEVs ($n=49$); 2) a group with mild GEVs (grade F1 and no red-color sign; $n=30$); and 3) a group with severe GEVs (grades F2–F3 or the presence of the red-color sign; $n=14$). Interventional treatment was recommended for patients with severe GEVs.

MRE and Stiffness Measurement

MRI examination was performed in all subjects after fasting for at least 3 hours to avoid the confounding effects of an overestimated stiffness value (26) and increased mesenteric blood flow after a meal (27). A 1.5 T MRI scanner (Signa, GE Healthcare, Milwaukee, WI) was used for all MRI tests. MRE was performed using a cylindrical passive driver to deliver transcostal vibrations, which was placed across the patient's right anterior chest wall for LS measurement and across the left posterolateral chest wall for SS measurement (28). The generator, placed outside the MRI examination room, produced a pneumatic vibration that was delivered to the passive driver via a plastic cylinder. The generator and passive driver were developed at the Mayo Clinic (Rochester, MN).

A breath-hold 2D gradient-echo MRE sequence was used to acquire two axial wave images. Our imaging parameters for MRE are shown in Table 1. The total acquisition time was 64 seconds (four 16-sec breath-

holds). The same MRE parameters were used for the liver and spleen. The MRI scanner automatically generated liver and spleen elastograms by processing the acquired propagating shear wave images using a previously described 2D direct inversion algorithm (29). The shear stiffness (kPa) of the tissue was presented as a pixel map.

The regions of interest (ROIs) were selected in the right lobe of the liver and near the surface of the spleen on the respective elastograms. In each ROI, the MRE slice proximal to the center of the passive driver on the chest wall was chosen for evaluation. As a rule, the ROIs were 1.0–1.5 cm^2 in area and placed near the edge of the liver or spleen next to the passive driver, where the penetrating wave was well-visualized and no interference was observed in the phase image. LS and SS were measured separately and independently by two radiologists (with 10 and 12 years of experience in abdominal radiology) who were blinded to clinical data and results of upper endoscopy. They selected two ROIs on the respective elastograms, and the average value of the results was used as the respective reviewer's stiffness values.

PC-MRI and Flow Measurements

Coronal slices (4-mm thickness) of steady-state acquisition images of the portal venous system were obtained for reference. All patients underwent breath-hold 2D PC-MRI for flow measurements in the PV. The slice acquired was a cross-section perpendicular to the flow of the PV. Our imaging parameters for PC-MRI are shown in Table 1. We chose velocity encoding of 30 cm/s for the measurement of the PV flow because the recently reported mean and maximum velocity of the PV were about 10 cm/s and 20 cm/s, respectively (30,31). Images were obtained with prospective cardiac gating using a pulse oximeter probe placed on the finger tip. The ROI was selected by a radiologist (7 years of experience in abdominal radiology) first on the magnitude image, and then it was copied onto the phase image. The mean velocity (V, cm/s), area (S, mm^2), and flow volume (Q, mL/min) of the PV were calculated using a workstation software (Advantage Workstation, GE Healthcare). The flow volume per minute was calculated by integrating over the flow volume during a cardiac cycle and multiplying by the number of heartbeats.

Splenic Volume Measurement

Splenomegaly has been observed as a major manifestation of PH and evaluated by a clinical manipulation and various cross-sectional imaging methods. We measured the spleen volume because of its possible association with the presence of GEVs; an abdominal radiologist who was blinded to clinical data and imaging findings measured the spleen volume in all subjects on fast spin echo T2-weighted images (imaging parameters were as follows: TR/TE 8000/65 msec, field of view 32 × 28, imaging matrix 256 × 192, slice thickness of 6 mm [no intersection gap], echo train length of 16), which was performed as a routine MRI examination in our institution. Spleen volume was estimated by using the following formula (32):

$$\text{spleen volume} = 0.524 \times W \times T \times L \ (cm^3)$$

where W and T are the maximum width (cm) and thickness (cm) of the spleen measured on the maximum cross-section, respectively, and L is the craniocaudal length (cm) of the spleen.

Biochemical Marker of Liver Fibrosis

The APRI was used as a blood-based marker of liver fibrosis. It was calculated using the following formula (11):

$$\text{APRI} = (\text{AST level}/\text{upper limit of AST}/\text{platelet count}/10^6 \times 100)$$

where the upper limit of AST was set at 32 IU/L, which was the reference value of our institutional laboratory. AST increases and platelet count decreases as hepatic fibrosis develops; therefore, the APRI can amplify the reverse relationship between the stage of liver fibrosis and AST level and platelet count (11).

Statistical Analysis

Interreader variability of the LS and SS values measured by the two reviewers was assessed using Pearson's correlation coefficient analysis. Both measurements showed good interreader reproducibility; therefore, we used an average value of the two results as a respective liver and spleen stiffness value in the subsequent analysis.

A univariate analysis in all study groups was performed using the Kruskal–Wallis test or chi-square test for patient characteristics (age, sex, BMI, and Child-Pugh grade), LS (using MRE and APRI), SS (using MRE), spleen volume, and flow-related parameters. A multivariate analysis was performed to discriminate any GEVs from no GEVs and severe GEVs from no GEVs or mild GEVs using a logistic regression model. Before the multivariate analysis, collinearity was assessed by calculating the correlation coefficient between the variables. A receiver operating characteristic (ROC) analysis was performed to estimate the efficacy of discrimination. The cutoff value for liver and spleen stiffness values were defined by the maximum positive and negative likelihood ratios. All statistical analyses were performed using the JMP software v. 9 (SAS Institute Japan, Tokyo, Japan) with the statistical significance for all analyses set at $P < 0.05$.

RESULTS

Patient Characteristics

No statistically significant differences in age, BMI, sex, or Child-Pugh grade were found between the three groups (Table 2).

Interreader Variability

Pearson's correlation coefficients of LS and SS measurements were 0.872 and 0.898, respectively.

Table 2
Comparison of Clinical Characteristics and Measured Parameters Between the Study Groups

	No GEVs $n=49$	Mild GEVs $n=30$	Severe GEVs $n=14$	P value
Age (years)	68 ± 8	70 ± 9	71 ± 6	0.261
M:F	34:15	19:11	6:8	0.713
BMI (kg/m^2)	19 ± 6	23 ± 8	18 ± 7	0.206
Child-Pugh A/B/C	42/7/0	22/7/1	10/3/1	0.362
MRE				
Liver stiffness (kPa)	4.0 ± 1.4	5.6 ± 2.3	6.1 ± 1.6	0.001
Spleen stiffness (kPa)	6.5 ± 2.1	8.5 ± 2.9	9.8 ± 1.7	0.001
APRI	1.4 ± 2.1	3.8 ± 2.4	2.0 ± 0.5	0.001
PC-MRI				
V_{PV} (cm/s)	8.6 ± 1.5	7.9 ± 1.8	7.5 ± 1.8	0.047
S_{PV} (mm^2)	135 ± 42	160 ± 51	147 ± 55	0.067
Q_{PV} (mL/min)	691 ± 264	765 ± 334	631 ± 298	0.515
Spleen volume (cm^3)	157 ± 76	240 ± 128	240 ± 81	0.005

Values are shown as the mean ± standard deviation.
GEV = gastroesophageal varices, BMI = body mass index, V_{PV} = mean portal vein velocity, S_{PV} = portal vein cross-sectional area, Q_{PV} = portal vein flow volume, APRI = aspartate aminotransferase-to-platelet ratio index.

Therefore, we used an average value of the two reviewer's results as a respective liver and spleen stiffness value in the subsequent analysis.

Results of Each Variable: Univariate Analysis

There were significant differences between the three groups in LS, APRI, and spleen volume. A significant difference was also observed in SS measurements, with the highest SS observed in the groups with severe GEVs (Table 2, Fig. 1). Of the PV flow measurements, only mean velocity (V_{PV}) showed a significant difference between the three groups.

Independent Associations: Multivariate Analysis

Moderate collinearity was observed between SS and spleen volume (correlation coefficient, 0.64) but not between any of the other parameters in a multiple regression model. In the multivariate analysis for discriminating any GEVs (mild or severe) from no GEVs, if both SS and spleen volume were included in a model, neither parameter showed a significant association ($P > 0.05$). When SS and spleen volume were included in a model separately, both parameters showed significant associations with the presence of any GEVs ($P = 0.018$ for SS, and 0.016 for spleen volume). Therefore, we chose both parameters as independent associators. LS, SS, and spleen volume showed independent associations with odds ratios (ORs) of 1.52, 1.35, and 1.01, respectively (Table 3). Areas under the ROC curve (AUC) for predicting any GEVs were 0.75 for LS, 0.76 for SS, and 0.73 for spleen volume. In the multivariate analysis for discriminating severe GEVs from no GEVs or mild GEVs, only SS showed a significant association (OR, 1.82) with an AUC of 0.81 (Table 3). Whether spleen volume was included or excluded, this result was stable. MRE of the liver and spleen and endoscopic findings of representative cases from the three groups are shown in Fig. 2.

Cutoff Values

Cutoff values with the maximum positive likelihood ratio for discriminating any GEVs from no GEVs were

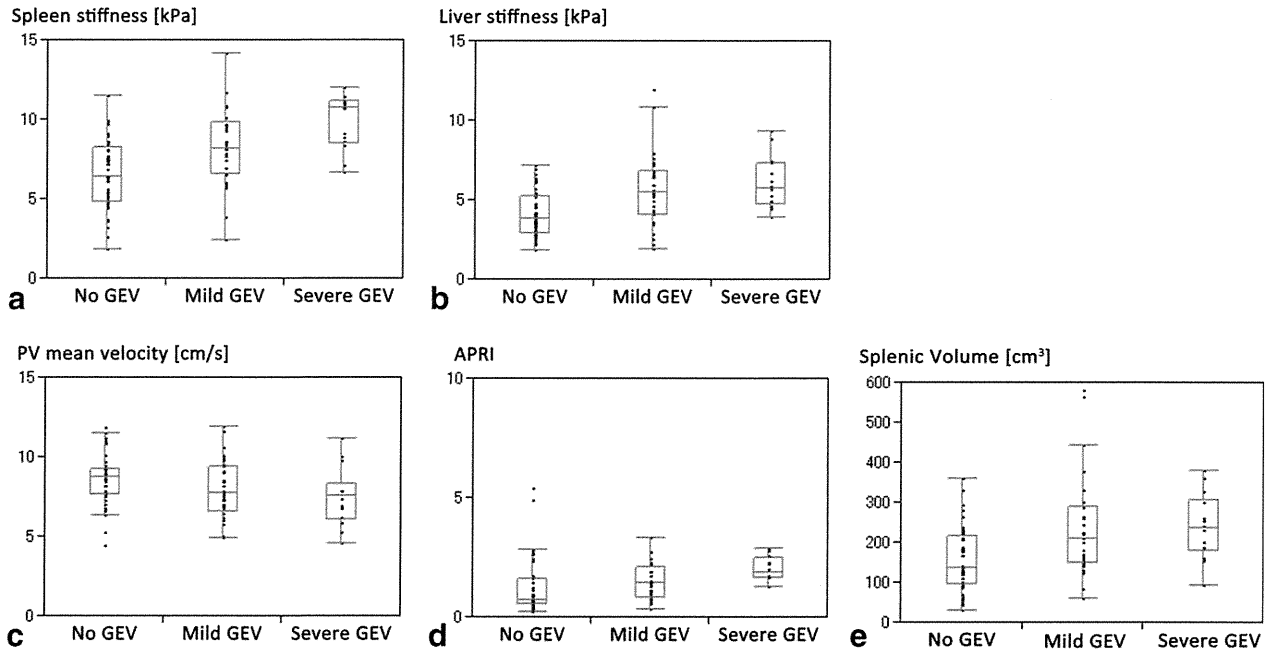

Figure 1. Box-and-whiskers plots of (a) spleen stiffness, (b) liver stiffness, (c) mean portal vein velocity, (d) APRI, and (e) spleen volume. The middle line in the box shows the median, the bottom and top lines of the box show the 25th and 75th percentiles, and the upper and lower whiskers show the minimum and maximum values. [Color figure can be viewed in the online issue, which is available at wileyonlinelibrary.com.]

Table 3
Multivariate Analysis for Discrimination of Any GEVs From No GEVs and Severe GEVs From No or Mild GEVs

	Diagnosis of any (mild and severe) GEVs			Diagnosis of severe GEVs		
	OR	95% CI	*P* value	OR	95% CI	*P* value
Spleen stiffness (kPa)	1.25	1.04–1.68	0.018	1.82	1.25–2.95	0.005
Liver stiffness (kPa)	1.52	1.13–2.17	0.006	1.42	0.96–2.61	0.078
V_{PV} (cm/s)	0.77	0.56–1.05	0.106	0.69	0.44–1.08	0.144
APRI	0.99	0.78–1.26	0.919	0.84	0.42–1.14	0.254
Spleen volume (cm^3)	1.01	1.00–1.01	0.016	0.99	0.98–1.01	0.809

GEVs = gastroesophageal varices, V_{PV} = mean portal vein velocity, OR = odds ratio, CI = confidence interval, APRI = aspartate aminotransferase platelet ratio index.

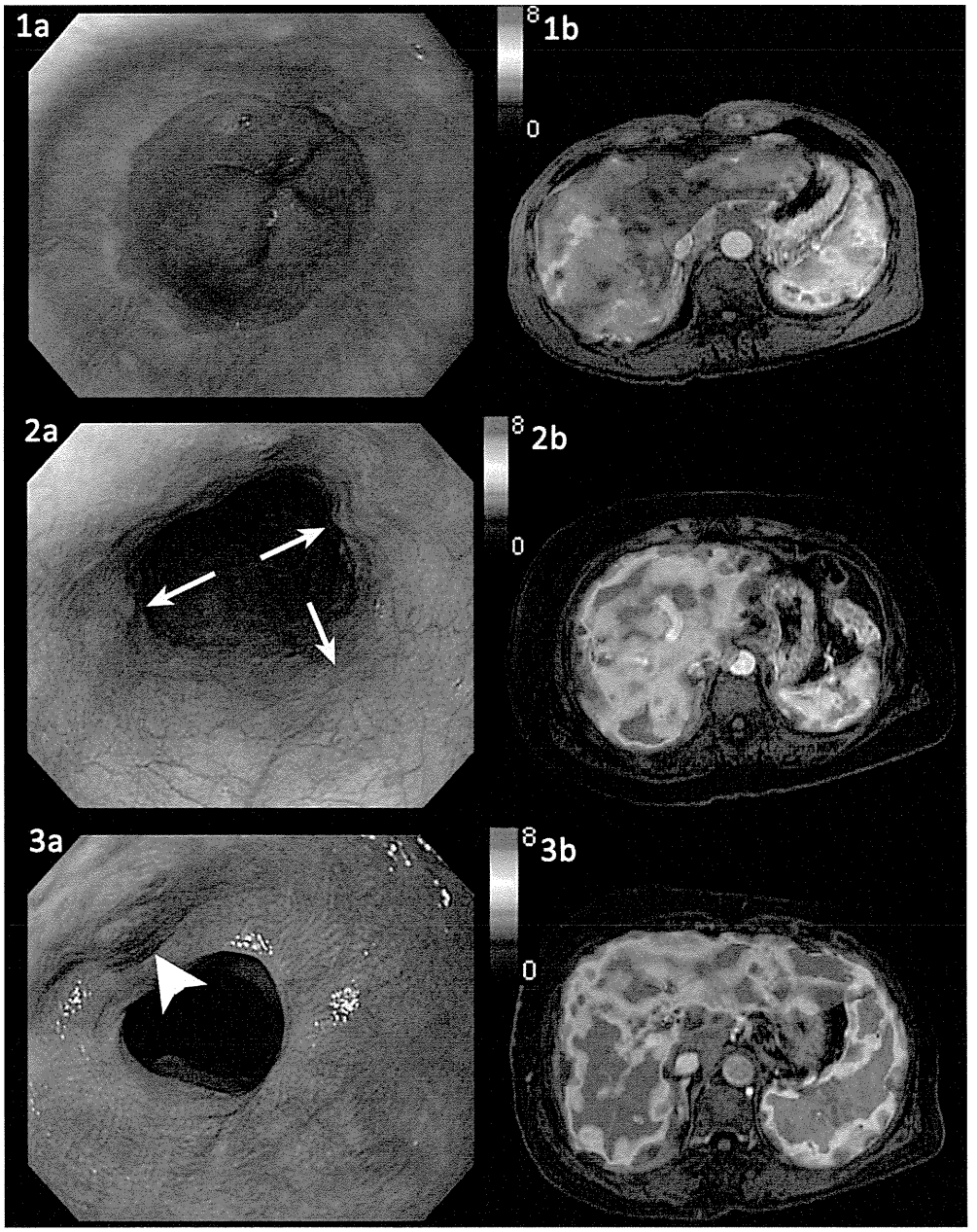

Figure 2. Case 1: A 53-year-old man with CLD without any GEVs (**1a**); liver and spleen elastograms superimposed on a contrast-enhanced MR image (**1b**) show low values for both liver (2.7 kPa) and spleen stiffness (4.7 kPa). Case 2: A 73-year-old woman with CLD with mild GEVs (**2a**, arrows); liver and spleen elastograms superimposed on a contrast-enhanced MR image (**2b**) show a high value for liver stiffness (6.4 kPa), but spleen stiffness remains low (6.6 kPa). Case 3: A 75-year-old woman with CLD with severe GEVs accompanied by the red-color sign (**3a**, arrowhead); liver and spleen elastograms superimposed on a contrast-enhanced MR image (**3b**) show high values for both liver (7.3 kPa) and spleen stiffness (12.0 kPa).

Table 4
Liver and Spleen Stiffness Cut-Off Values for Discriminating Any GEVs From No GEVs and Severe GEVs From No or Mild GEVs

Cut-off value	Sensitivity	Specificity	PPV	NPV	LR+	LR–
Diagnosis of any (mild and severe) GEVs						
Spleen stiffness						
10.1 kPa	34% (15/44)	98% (48/49)	94% (15/16)	62% (48/77)	16.70	1.48
5.6 kPa	95% (42/44)	41% (20/49)	59% (42/71)	91% (20/22)	1.61	8.98
Liver stiffness						
6.7 kPa	29% (13/44)	96% (47/49)	86% (13/15)	60% (47/78)	7.23	1.36
3.4 kPa	91% (40/44)	35% (17/49)	55% (40/72)	81% (17/21)	1.39	3.81
Diagnosis of severe GEVs						
Spleen stiffness						
10.8 kPa	43% (6/14)	95% (75/79)	60% (6/10)	90% (75/83)	8.46	1.66
7.1 kPa	93% (13/14)	45% (35/79)	23% (13/57)	97% (35/36)	1.67	6.20
Liver stiffness						
8.8 kPa	14% (2/14)	98% (77/79)	50%(2/4)	87% (77/89)	5.64	1.14
4.4 kPa	93% (13/14)	52% (41/79)	25% (13/51)	98% (41/42)	1.93	7.27

PPV = positive predictive value, NPV = negative predictive value, LR+ = positive likelihood ratio, LR– = negative likelihood ratio.

10.1 kPa for SS and 6.7 kPa for LS. These cutoff values provided positive predictive values of 94% and 86% for SS and LS, respectively. Maximum negative likelihood ratios were observed with the cutoff values of 5.6 kPa for SS and 3.4 kPa for LS, which resulted in negative predictive values of 91% and 81%, respectively (Table 4).

To distinguish severe GEVs from no or mild GEVs, the maximum positive likelihood ratios were 10.8 kPa for SS and 8.8 kPa for LS, whereas the maximum negative likelihood ratios were obtained with a cutoff value of 7.1 kPa for SS and 4.4 kPa for LS (Table 4).

DISCUSSION

Various factors associated with the development and progression of GEVs have been suggested in patients with cirrhosis and chronic hepatitis (33). Among those factors, liver fibrosis grade, which has been reported to be correlated with LS measured by MRE (19,34), is an important marker of PH and GEVs. In our study, both markers of liver fibrosis, LS and the APRI, were correlated with the severity of GEVs. LS was an independent predictor of mild-to-severe GEVs, which is consistent with the previous studies using ultrasound elastography (3,35) and MR elastography (24). The APRI was not a significant indicator of GEVs, which is also consistent with a recent study (36). Meanwhile, it has been recently reported that the hepatic venous pressure gradient is better correlated with SS than with LS measured by transient elastography (14). The results of the multivariate analyses in our study are in line with the previous reports. Although the precise mechanisms leading to spleen enlargement in PH are poorly understood, splenic congestion has been suggested to play a major role in increasing spleen volume, which is observed in neoangiogenesis and lymphoid hyperplasia in the spleen (13,37). The reason why the stiffness is increased in PH can be explained by increased tissue perfusion; a recent study using a pig model of renal ischemia suggested that decreased perfusion reduced tissue stiffness (38). In a previous study, the mean SS measured by MRE in healthy volunteers was 4.2 kPa (28). In our study, the SS in patients with CLD without GEVs was higher (6.7 kPa) than the previously reported data, indicating that SS might increase in the precirrhotic stage. Although SS was more reliable than the other MRI-based parameters in the assessment of GEVs in our study, a significant overlap between the three groups in SS value was observed. Therefore, we conclude that SS alone cannot be used as an indicator of GEVs and more reliable noninvasive methods should be developed and validated.

We also demonstrated that spleen volume was significantly different among the three groups studied. In the multivariate analysis, spleen volume showed significant association with the presence of any GEVs, but no significant association with severe GEVs. A recent study showed that spleen volume combined with a biochemical marker (eg, platelet count and/or albumin) can predict the presence of varices in patients with CLD (39). Meanwhile, in pediatric patients with extrahepatic portal vein obstruction, spleen volume does not correlate with the grade of varices (40). We speculate that spleen volume will increase with PH development; however, it might not be useful by itself for the assessment of severe GEVs.

We showed excellent interreader variability for both LS and SS measurements. Of these, the reproducibility of LS was consistent with a recent report (41). To our best knowledge, the reproducibility of SS measurement has not been reported so far. Although we did not assess the repeatability of stiffness measurements in our study, a previous report showed excellent repeatability of MRE of the liver. (17,18,41). In our institution, clinical technicians are proficient in the MRE technique and all procedures are conducted without complications. MRE is associated with only slight pneumatic vibration and rarely causes subjective discomfort or pain. Recently, gadoxetic acid-enhanced MRI has become a popular method in patients with cirrhosis to assess hepatocellular carcinoma and a 20-minute waiting period for hepatocyte phase image is sufficient to obtain an MRE image. In

our opinion, MRE of the liver and spleen is well-tolerated by almost all patients and should be implemented as part of a routine MRI examination.

Ultrasound parameters such as LS, SS, and spleen size have been widely investigated and reported to be reliable indicators of GEVs (3–8). Ultrasound methods are widely available and inexpensive but they are operator-dependent and less sensitive, especially in obese patients.

In this study we did not assess the visually detectable GEVs on routine MRI because the focus of this study was also on quantitative parameters rather than qualitative assessments, which might be inferior in reproducibility. Furthermore, our study cohort comprised a heterogeneous group in which both patients with and without contrast-enhanced MRI were included. This heterogeneity of contrast-enhanced MRI might influence reliability of diagnostic performance of visually detectable GEVs on MRI (10). In simple assessment by one author of this study, visually detectable GEVs on routine MRI, which was defined as dilated luminal vessels abutting or protruding into the luminal space (23), were observed in three patients with mild GEVs, nine patients with severe GEVs, and not observed in no GEVs. Sensitivity and specificity were 27% (12/44), 100% (49/49) for any GEVs, and 64% (9/14), 96% (76/79) for severe GEVs, respectively. These results of visual assessment were comparable with the results of SS.

PV flow measurements by PC-MRI and duplex Doppler ultrasound in the previous studies showed inconclusive results for assessing PH and GEVs (23,42). The results of our study also suggest that PV flow measurements are less promising for predicting GEVs than SS. This may be due to complex contributing factors such as meal consumption prior to examination, cardiac output, and breath-holding (43), in addition to the inherent instability in measurements by 2D PC-MRI. The recently developed time-resolved 3D PC-MRI or 4D PC-MRI may provide a more comprehensive assessment of PV flow dynamics (44).

Our study has several limitations. First, the cutoff values were based on the retrospective patient cohort; therefore, they could not be directly extrapolated to clinical practice, and further prospective studies are needed to validate these values for the prediction of GEVs. Second, there is no available reference standard for SS or PH. Therefore, the validity and robustness of the SS measurement could not be verified. Third, the time between MRI and upper endoscopy was relatively long and differed between patients, which might have produced biased results. Finally, we could not set the endpoint of bleeding from GEVs, which is the most important clinical outcome. Prospective observation should be conducted to elucidate the utility of noninvasive functional MRI parameters in clinical settings.

In conclusion, MRE of the liver and spleen, and spleen volume measured on routine MRI, are useful for predicting GEVs in patients with CLD. Spleen stiffness is a more reliable predictor of severe GEVs than liver stiffness and spleen volume.

ACKNOWLEDGMENTS

We thank Richard Ehman and Scott Kruse from the Mayo Clinic for providing the MRE system and Tetsuya Wakayama from GE Healthcare for setting up the equipment. We also appreciate tremendous support for the research by the doctors in the 1st Department of Internal Medicine and the 1st Department of Surgery, University of Yamanashi.

REFERENCES

1. Garcia-Tsao G, Bosch J. Management of varices and variceal hemorrhage in cirrhosis. N Engl J Med 2010;362:823–832.
2. de Franchis R. Revising consensus in portal hypertension: report of the Baveno V consensus workshop on methodology of diagnosis and therapy in portal hypertension. J Hepatol 2010;53:762–768.
3. Kim BK, Han KH, Park JY, et al. A liver stiffness measurement-based, noninvasive prediction model for high-risk esophageal varices in B-viral liver cirrhosis. Am J Gastroenterol 2010;105: 1382–1390.
4. Baig WW, Nagaraja MV, Varma M, Prabhu R. Platelet count to spleen diameter ratio for the diagnosis of esophageal varices: is it feasible? Can J Gastroenterol 2008;22:825–828.
5. Sarangapani A, Shanmugam C, Kalyanasundaram M, Rangachari B, Thangavelu P, Subbarayan JK. Noninvasive prediction of large esophageal varices in chronic liver disease patients. Saudi J Gastroenterol 2010;16:38–42.
6. Plestina S, Pulanic R, Kralik M, Samarzija M. Color Doppler ultrasonography is reliable in assessing the risk of esophageal variceal bleeding in patients with liver cirrhosis. Wien Klin Wochenschr 2005;117:711–717.
7. Berzigotti A, Gilabert R, Abraldes JG, et al. Noninvasive prediction of clinically significant portal hypertension and esophageal varices in patients with compensated liver cirrhosis. Am J Gastroenterol 2008;103:1159–1167.
8. Joseph T, Madhavan M, Devadas K, Ramakrishnannair VK. Doppler assessment of hepatic venous waves for predicting large varices in cirrhotic patients. Saudi J Gastroenterol 2011;17:36–39.
9. Kim YJ, Raman SS, Yu NC, To'o KJ, Jutabha R, Lu DS. Esophageal varices in cirrhotic patients: evaluation with liver CT. AJR Am J Roentgenol 2007;188:139–144.
10. Goshima S, Kanematsu M, Kondo H, et al. Detection and grading for esophageal varices in patients with chronic liver damage: comparison of gadolinium-enhanced and unenhanced steady-state coherent MR images. Magn Reson Imaging 2009;27:1230–1235.
11. Wai CT, Greenson JK, Fontana RJ, et al. A simple noninvasive index can predict both significant fibrosis and cirrhosis in patients with chronic hepatitis C. Hepatology 2003;38:518–526.
12. Reiberger T, Ferlitsch A, Payer BA, et al. Noninvasive screening for liver fibrosis and portal hypertension by transient elastography-a large single center experience. Wien Klin Wochenschr 2012;124:395–402.
13. Bolognesi M, Merkel C, Sacerdoti D, Nava V, Gatta A. Role of spleen enlargement in cirrhosis with portal hypertension. Dig Liver Dis 2002;34:144–150.
14. Hirooka M, Ochi H, Koizumi Y, et al. Splenic elasticity measured with real-time tissue elastography is a marker of portal hypertension. Radiology 2011;261:960–968.
15. Colecchia A, Montrone L, Scaioli E, et al. Measurement of spleen stiffness to evaluate portal hypertension and the presence of esophageal varices in patients with HCV-related cirrhosis. Gastroenterology 2012;143:646–654.
16. Huwart L, Sempoux C, Vicaut E, et al. Magnetic resonance elastography for the noninvasive staging of liver fibrosis. Gastroenterology 2008;135:32–40.
17. Hines CD, Bley TA, Lindstrom MJ, Reeder SB. Repeatability of magnetic resonance elastography for quantification of hepatic stiffness. J Magn Reson Imaging 2010;31:725–731.
18. Shire NJ, Yin M, Chen J, et al. Test-retest repeatability of MR elastography for noninvasive liver fibrosis assessment in hepatitis C. J Magn Reson Imaging 2011;34:947–955.
19. Ichikawa S, Motosugi U, Ichikawa T, et al. Magnetic resonance elastography for staging liver fibrosis in chronic hepatitis C. Magn Reson Med Sci 2012;11:291–297.

20. Talwalkar JA, Yin M, Venkatesh S, et al. Feasibility of in vivo MR elastographic splenic stiffness measurements in the assessment of portal hypertension. AJR Am J Roentgenol 2009;193:122–127.
21. Nedredal GI, Yin M, McKenzie T, et al. Portal hypertension correlates with splenic stiffness as measured with MR elastography. J Magn Reson Imaging 2011;34:79–87.
22. Yin M, Kolipaka A, Woodrum DA, et al. Hepatic and splenic stiffness augmentation assessed with MR elastography in an in vivo porcine portal hypertension model. J Magn Reson Imaging 2013; 36:809–815.
23. Gouya H, Vignaux O, Sogni P, et al. Chronic liver disease: systemic and splanchnic venous flow mapping with optimized cine phase-contrast MR imaging validated in a phantom model and prospectively evaluated in patients. Radiology 2011;261:144–155.
24. Morisaka H, Motosugi U, Ichikawa T, et al. MR-based measurements of portal vein flow and liver stiffness for predicting gastroesophageal varices. Magn Reson Med Sci 2013;12:77–86.
25. Tajiri T, Yoshida H, Obara K, et al. General rules for recording endoscopic findings of esophagogastric varices (2nd ed.). Dig Endosc 2010;22:1–9.
26. Yin M, Talwalkar JA, Glaser KJ, et al. Dynamic postprandial hepatic stiffness augmentation assessed with MR elastography in patients with chronic liver disease. AJR Am J Roentgenol 2011; 197:64–70.
27. Tsukuda T, Ito K, Koike S, et al. Pre- and postprandial alterations of portal venous flow: evaluation with single breath-hold three-dimensional half-Fourier fast spin-echo MR imaging and a selective inversion recovery tagging pulse. J Magn Reson Imaging 2005;22:527–533.
28. Mannelli L, Godfrey E, Joubert I, et al. MR elastography: spleen stiffness measurements in healthy volunteers—preliminary experience. AJR Am J Roentgenol 2010;195:387–392.
29. Manduca A, Oliphant TE, Dresner MA, et al. Magnetic resonance elastography: non-invasive mapping of tissue elasticity. Med Image Anal 2001;5:237–254.
30. Stankovic Z, Frydrychowicz A, Csatari Z, et al. MR-based visualization and quantification of three-dimensional flow characteristics in the portal venous system. J Magn Reson Imaging 2010;32:466–475.
31. Stankovic Z, Csatari Z, Deibert P, et al. Normal and altered three-dimensional portal venous hemodynamics in patients with liver cirrhosis. Radiology 2012;262:862–873.
32. Yetter EM, Acosta KB, Olson MC, Blundell K. Estimating splenic volume: sonographic measurements correlated with helical CT determination. AJR Am J Roentgenol 2003;181:1615–1620.
33. Fontana RJ, Sanyal AJ, Ghany MG, et al. Factors that determine the development and progression of gastroesophageal varices in patients with chronic hepatitis C. Gastroenterology 2010;138: 2321–2331, 2331 e2321–2322.
34. Huwart L, Sempoux C, Salameh N, et al. Liver fibrosis: noninvasive assessment with MR elastography versus aspartate aminotransferase-to-platelet ratio index. Radiology 2007;245:458–466.
35. Vizzutti F, Arena U, Romanelli RG, et al. Liver stiffness measurement predicts severe portal hypertension in patients with HCV-related cirrhosis. Hepatology 2007;45:1290–1297.
36. Zambam de Mattos A, Alves de Mattos A, Daros LF, Musskopf MI. Aspartate aminotransferase-to-platelet ratio index (APRI) for the non-invasive prediction of esophageal varices. Ann Hepatol 2013; 12:810–814.
37. Mejias M, Garcia-Pras E, Gallego J, Mendez R, Bosch J, Fernandez M. Relevance of the mTOR signaling pathway in the pathophysiology of splenomegaly in rats with chronic portal hypertension. J Hepatol 2010;52:529–539.
38. Warner L, Yin M, Glaser KJ, et al. Noninvasive In vivo assessment of renal tissue elasticity during graded renal ischemia using MR elastography. Invest Radiol 2011;46:509–514.
39. Min YW, Bae SY, Gwak GY, et al. A clinical predictor of varices and portal hypertensive gastropathy in patients with chronic liver disease. Clin Mol Hepatol 2012;18:178–184.
40. Singh IK, Bhatnagar V, Gupta AK, Seith A. Correlation of splenic volume with hematological parameters, splenic vein diameter, portal pressure and grade of varices in extrahepatic portal vein obstruction in children. Pediatr Surg Int 2011;27:467–471.
41. Lee YJ, Lee JM, Lee JE, et al. MR elastography for noninvasive assessment of hepatic fibrosis: reproducibility of the examination and reproducibility and repeatability of the liver stiffness value measurement. J Magn Reson Imaging 2013 [Epub ahead of print].
42. Li FH, Hao J, Xia JG, Li HL, Fang H. Hemodynamic analysis of esophageal varices in patients with liver cirrhosis using color Doppler ultrasound. World J Gastroenterol 2005;11:4560–4565.
43. Burkart DJ, Johnson CD, Reading CC, Ehman RL. MR measurements of mesenteric venous flow: prospective evaluation in healthy volunteers and patients with suspected chronic mesenteric ischemia. Radiology 1995;194:801–806.
44. Francois CJ, Srinivasan S, Schiebler ML, et al. 4D cardiovascular magnetic resonance velocity mapping of alterations of right heart flow patterns and main pulmonary artery hemodynamics in tetralogy of Fallot. J Cardiovasc Magn Reson 2012;14:16.

Original Article

Changes in Plasma Vascular Endothelial Growth Factor at 8 Weeks After Sorafenib Administration as Predictors of Survival for Advanced Hepatocellular Carcinoma

Kaoru Tsuchiya, MD, PhD[1]; Yasuhiro Asahina, MD, PhD[2,3]; Shuya Matsuda, MD[1]; Masaru Muraoka, MD[1]; Toru Nakata, MD[1]; Yuichiro Suzuki, MD[1]; Nobuharu Tamaki, MD[1]; Yutaka Yasui, MD[1]; Shoko Suzuki, MD[1]; Takanori Hosokawa, MD[1]; Takashi Nishimura, MD, PhD[1]; Ken Ueda, MD[1]; Teiji Kuzuya, MD, PhD[1]; Hiroyuki Nakanishi, MD, PhD[1]; Jun Itakura, MD, PhD[1]; Yuka Takahashi, MD, PhD[1]; Masayuki Kurosaki, MD, PhD[1]; Nobuyuki Enomoto, MD, PhD[4]; and Namiki Izumi, MD, PhD[1]

BACKGROUND: A new predictive biomarker for determining prognosis in patients with hepatocellular carcinoma (HCC) who receive sorafenib is required, because achieving a reduction in tumor size with sorafenib is rare, even in patients who have a favorable prognosis. Vascular endothelial growth factor (VEGF) receptor is a sorafenib target. In the current study, the authors examined changes in plasma VEGF concentrations during sorafenib treatment and determined the clinical significance of VEGF as a prognostic indicator in patients with HCC. **METHODS:** Plasma VEGF concentrations were serially measured in 63 patients with advanced HCC before and during sorafenib treatment. A plasma VEGF concentration that decreased >5% from the pretreatment level at 8 weeks was defined as a "VEGF decrease." An objective tumor response was determined using modified Response Evaluation Criteria in Solid Tumors 1 month after the initiation of therapy and every 3 months thereafter. **RESULTS:** Patients who had a VEGF decrease at week 8 (n = 14) had a longer median survival than those who did not have a VEGF decrease (n = 49; 30.9 months vs 14.4 months; $P = .038$). All patients who had a VEGF decrease survived for >6 months, and the patients who had both a VEGF decrease and an α-fetoprotein response (n = 6) survived during the observation period (median, 19.7 months; range, 6.5-31.0 months). In univariate analyses, a VEGF decrease, radiologic findings classified as progressive disease, and major vascular invasion were associated significantly with 1-year survival; and, in multivariate analysis, a VEGF decrease was identified as an independent factor associated significantly with survival. **CONCLUSIONS:** A plasma VEGF concentration decrease at 8 weeks after starting sorafenib treatment may predict favorable overall survival in patients with advanced HCC. ***Cancer* 2014;120:229-37.** © 2013 The Authors. *Cancer* published by Wiley Periodicals, Inc. on behalf of American Cancer Society. This is an open access article under the terms of the Creative Commons Attribution-NonCommercial-NoDerivs License, which permits use and distribution in any medium, provided the original work is properly cited, the use is non-commercial and no modifications or adaptations are made.

KEYWORDS: antiangiogenic therapy, biomarker, hepatocellular carcinoma, prognosis, α-fetoprotein.

INTRODUCTION

Hepatocellular carcinoma (HCC) is the most common primary malignancy of the liver (70%-85%) and a major cause of mortality. It is the fifth and seventh most frequent cancer and the second and sixth most frequent cause of cancer death in men and women, respectively.[1] At early stages or at Barcelona Clinic Liver Cancer stage A, a 5-year survival rate of 60% to 70% can be achieved in well selected patients with HCC who undergo surgical therapies (liver resection or transplantation) or locoregional procedures (ie, radiofrequency ablation).[2] However, treatment of advanced HCC that is not amenable to surgical or locoregional therapies remains a challenge in clinical practice.

Sorafenib is an oral, small-molecule tyrosine kinase inhibitor that blocks the synthesis of several intracellular proteins considered to be important for tumor progression, including the platelet-derived growth factor receptor beta, raf kinase, and the vascular endothelial growth factor (VEGF) receptor. VEGF is a homodimetric glycoprotein with a molecular weight of 45 kDa. The VEGF family includes VEGF-A, VEGF-B, VEGF-C, VEGF-D, and a structurally related molecule: placental growth factor. Three high-affinity VEGF tyrosine kinase receptors (VEGFRs) have been identified:

Corresponding author: Namiki Izumi, MD, PhD, Department of Gastroenterology and Hepatology, Musashino Red Cross Hospital, 1-26-1 Kyonan-cho, Musashino-shi, Tokyo 180-8610, Japan; Fax: (011) 81-422-32-9551; nizumi@musashino.jrc.or.jp

[1]Department of Gastroenterology and Hepatology, Musashino Red Cross Hospital, Tokyo, Japan; [2]Department of Gastroenterology and Hepatology, Tokyo Medical and Dental University, Tokyo, Japan; [3]Department of Liver Disease Control, Tokyo Medical and Dental University, Tokyo, Japan; [4]First Department of Internal Medicine, University of Yamanashi, Yamanashi, Japan

The first 2 authors contributed equally to this article.

DOI: 10.1002/cncr.28384, **Received:** April 2, 2013; **Revised:** August 10, 2013; **Accepted:** August 15, 2013, **Published online** October 7, 2013 in Wiley Online Library (wileyonlinelibrary.com)